Synthesis and Characterization of Homo- and Heterodinuclear Complexes Containing the $N_3M(\mu_2\text{-}SR)_3MN_3$ Core (M = Fe, Co, Ni)

Berthold Kersting,*,† Dieter Siebert,‡ Dirk Volkmer,§ Mario J. Kolm,† and Christoph Janiak†

Institut für Anorganische und Analytische Chemie, Universität Freiburg, Albertstrasse 21, D-79104 Freiburg, Germany, Institut für Physikalische Chemie, Universität Freiburg, Albertstrasse 23a, D-79104 Freiburg, Germany, and Fakultät für Chemie der Universität Bielefeld, Universitätsstrasse 25, D-33615 Bielefeld, Germany

Received January 15, 1999

A novel amine-thiolate ligand, H_3**3**·6HCl (*N*,*N*′,*N*″-tris-[2-thio-3-aminomethyl-5-*tert*-butylbenzyl]-1,1,1-tris-(aminomethyl)ethane), has been synthesized and used in the preparation of dinuclear complexes of Fe, Co, and Ni. The nonadentate N_6S_3 ligand H_3**3** is formally derived from the symmetric tridentate N_2S ligand H_1**1** (2,6-bis(aminomethyl)-4-*tert*-butylthiophenol). It provides two dissimilar octahedral N_3S_3 and N'_3S_3 coordination sites to give complexes with a central $N_3M(\mu_2\text{-}SR)_3MN'_3$ core structure (N and N′ denote primary and secondary amine nitrogen atoms, respectively). The complexes of H_3**3** exist as dinuclear $[M^{II}_2(\mathbf{3})]^+$, $[M^{III}M^{II}(\mathbf{3})]^{2+}$, or $[M^{III}_2(\mathbf{3})]^{3+}$ species which are all accessible by chemical or electrochemical reduction/oxidation. The following complexes were isolated as microcrystalline solids: $[Co^{III}_2(\mathbf{3})][ClO_4]_3$ (**4b**), $[Ni^{III}Ni^{II}(\mathbf{3})][BPh_4]_2$ (**5b**), and $[Fe^{III}Fe^{II}(\mathbf{3})][BPh_4]_2$ (**6b**). The chemical and physicochemical properties of the respective species are very similar to those of Fe, Co, and Ni complexes of H_1**1**, $[M_2(\mathbf{1})_3]^{n+}$ (M = Co, n = 3, (**4a**); M = Ni, n = 2 (**5a**); M = Fe, n = 2 (**6a**)), and support the formulation of **4b**−**6b** as discrete dinuclear species with a central $N_3M(\mu_2\text{-}SR)_3MN'_3$ core. NMR spectra of diamagnetic cobalt complexes **4a** and **4b** reveal the complexes to be C_{3h} and C_3 symmetric, respectively, in the solution state. The crystal structure determination of $[Co^{III}_2(\mathbf{1})_3][Fe(CN)_6]$·7MeOH·$3H_2O$ (**4c**) (monoclinic, space group *C*2/c, a = 28.037(2) Å, b = 17.861(1) Å, c = 25.727(2) Å, β = 90.24(1)°, and Z = 8) reveals **4c** to consist of dinuclear $[Co^{III}_2(\mathbf{1})_3]^{3+}$ trications featuring two *fac*-octahedral $N_3Co^{III}(SR)_3$ units bridged at the thiolate sulfur atoms. Compound **4c** represents the first structurally characterized M^{III}_2 complex of H_1**1**. The ability of H_3**3** to form heterodinuclear complexes is demonstrated with the synthesis of $[Co^{III}Ni^{II}(\mathbf{3})][BPh_4]_2$ (**7**) and its linkage isomer $[Ni^{II}Co^{III}(\mathbf{3})][BPh_4]_2$ (**8**). All complexes undergo two electrochemically and chemically reversible one-electron-transfer reactions which convert the respective $[M_2(\mathbf{3})]^{n+}$ species. For $M^{III}_2/M^{III}M^{II}$ ($E^1_{1/2}$) and $M^{III}M^{II}/M^{II}_2$ ($E^2_{1/2}$): −0.40 V, −0.84 V (M = Co), +0.49 V, +0.05 V (M = Ni), +0.21 V, −0.33 V (M = Fe) vs SCE. Heterodinuclear complexes **7** and **8** also give rise to two consecutive one-electron-transfer processes at $E^1_{1/2}$ ($Ni^{III/II}$) and $E^2_{1/2}$ ($Co^{III/II}$): +0.55 V, −0.71 V (for **7**) and +0.60 V, −0.86 V (for **8**), respectively. Comparison of the electrochemical properties of $[Co^{III}Ni^{II}(\mathbf{3})]^{2+}$ and $[Ni^{III}Ni^{II}(\mathbf{3})]^{2+}$ reveals the $Ni^{III/II}$ redox potential in the dinuclear complexes to be influenced by the oxidation state of the adjacent metal ion. At 77 K the mixed-valent $Ni^{III}Ni^{II}$ (S = $^3/_2$ spin ground states) and $Fe^{III}Fe^{II}$ complexes (S = $^1/_2$ spin ground states) exhibit localized and delocalized valencies, respectively, as indicated by UV−vis, EPR, and ^{57}Fe Mössbauer spectroscopy.

Introduction

Face-sharing bioctahedral complexes of the type $Y_3M(\mu_2\text{-}X)_3MY_3$ (Chart 1), where X and Y are single-atom bridging and single-atom terminal ligands, respectively, represent an extensively studied class of compounds,[1] since they display a variety of metal−metal interactions that can be studied at the molecular level.[2,3]

Generally, the nature of these interactions (bonding interactions, intramolecular exchange coupling phenomena) depends on several factors, as for instance the number of metal d electrons, the number of the row in the periodic table, and the bridging ligand X.[4] The role of the latter, for example, is studied in complexes of type II, where the bridging ligand X can be varied while the influence of the terminal ligands Y is held constant by use of a facially coordinating tridentate ligand. Such complexes are well-suited to study intramolecular exchange interactions between paramagnetic first-row transition metal ions as a function of their respective d^n electron configuration.[5,6] In

Chart 1

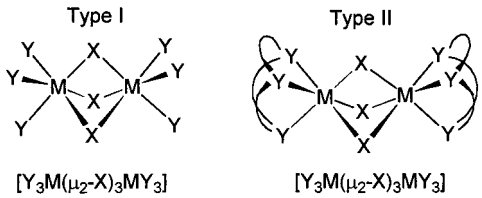

* Author to whom correspondence should be addressed (e-mail: kerstber@sun2.ruf.uni-freiburg.de).
† Institut für Anorganische und Analytische Chemie, Universität Freiburg.
‡ Institut für Physikalische Chemie, Universität Freiburg.
§ Fakultät für Chemie, Universität Bielefeld.

(1) Cotton, F. A.; Ucko, D. A. *Inorg. Chim. Acta* **1972**, *6*, 161−72.
(2) Summerville, R. H.; Hoffmann, R. *J. Am. Chem. Soc.* **1979**, *101*, 3821−31.
(3) Leuenberger, B.; Güdel, H. U. *Inorg. Chem.* **1986**, *25*, 181−8.
(4) Burstein, B. E.; Cotton, F. A.; Fang, A. *Inorg. Chem.* **1983**, *22*, 2127−33.
(5) Bossek, U.; Nühlen, D.; Bill, E.; Glaser, T.; Krebs, C.; Weyhermüller, T.; Wieghardt, K.; Lengen, M.; Trautwein, A. X. *Inorg. Chem.* **1997**, *36*, 2834−43.

10.1021/ic990087t CCC: $18.00
Published on Web 07/31/1999

certain cases, type II complexes allow for the preparation of mixed-valent species[7−10] with interesting magnetic properties.[11−12]

For di- and trivalent first-row transition metal ions most of the studies are focused on halide, hydroxide, or alkoxide as bridging ligands, whereas complexes bridged by three thiolate,[13] selenolate,[14] or tellurolate bridges are less well investigated.[15] This is true in particular for dinuclear complexes.[16−21] A recent example is (tacn)$Fe^{III}(S_2)_3Fe^{III}$(tacn) (tacn = 1,4,7-triazacyclononane), which has been reported by Rauchfuss et al.[22] Here the structural and magnetic properties suggest the existence of a direct Fe−Fe bond. Interestingly, certain enzymes also contain $M(\mu_2\text{-}S)_xM$ structures at their active sites,[23,24] as for instance the dinuclear $Fe(\mu_2\text{-}SR)_2(\mu_2\text{-}X)Ni$ assembly in [NiFe]-hydrogenase from *Desulfovibrio gigas*, although the nature of the third bridging atom X remains unknown at present.[25−27]

Recently we reported the syntheses and characterization of face-sharing bioctahedral Fe, Co,[28] and Ni[29] complexes $[M_2(\mathbf{1})_3]^{n+}$ of the symmetric amine-thiolate ligand $H_3\mathbf{1}$ (see Chart 2). It was anticipated that the amine−thiolate ligand $H_3\mathbf{3}$ would similarly allow for the preparation of dinuclear complexes $[M_2\mathbf{3}]^{n+}$ with a central $N_3M(\mu_2\text{-}SR)_3MN_3$ core structure. Moreover, because of its two dissimilar N_3S_3 and N'_3S_3 binding pockets,[30] this ligand was expected to support the formation of heterodinuclear complexes,[31] which were not accessible with $H_3\mathbf{1}$.

We here describe the synthesis of a series of dinuclear complexes with the new asymmetric N_6S_3 ligand $H_3\mathbf{3}$. The

Chart 2

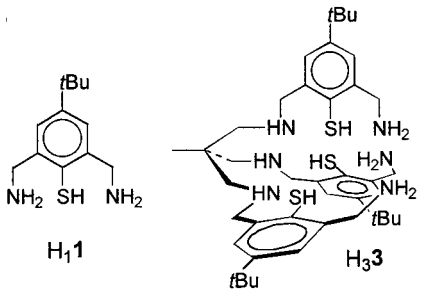

homodinuclear complexes $[M_2(\mathbf{3})]^{n+}$ (M = Fe, Co, and Ni) and the heterodinuclear complexes $[M'M(\mathbf{3})]^{n+}$ (M′ = Co or Ni, M = Ni or Co) are characterized by NMR and UV−vis spectroscopy and by cyclic voltammetry. The crystal structure of the complex $[Co_2(\mathbf{1})_3]^{3+}$ in $[Co_2(\mathbf{1})_3][Fe(CN)_6]$ is presented and compared with the solution-state structure of the complex $[Co_2(\mathbf{3})]^{3+}$ determined by two-dimensional ^{1}H NMR spectroscopy. The electrochemical properties of these complexes are discussed with respect to the influence of an adjacent metal ion M on the $Ni^{III/II}$ redox potential in $M(\mu_2\text{-}SR)_3Ni$ structures.[32−35] Preliminary EPR and ^{57}Fe Mössbauer data for the mixed-valent complexes are also presented.

Experimental Section

Preparation of Compounds. Unless noted otherwise, all operations were carried out under a pure dinitrogen atmosphere. Reagents were commercial samples and were not purified further. The compounds 1,1,1-tris(aminomethyl)ethane,[36] *tert*-butyl (4-*tert*-butyl-2-formyl-6-hydroximinomethylphenyl) sulfide,[37] and $[Co_2(\mathbf{1})_3][ClO_4]_3$ (**4a**)[38] were prepared according to published procedures. Solvents were predried over molecular sieves and freshly distilled from appropriate drying agents. **CAUTION!** *Transition metal perchlorates are hazardous and may explode. Only small quantities should be prepared and great care taken.*[39]

***N,N′,N″*-Tris[2-*tert*-butylsulfanyl-3-hydroximinomethyl-5-*tert*-butylbenzyl]-1,1,1-tris(aminomethyl)ethane (2).** A solution of 1,1,1-tris(aminomethyl)ethane (117 mg, 1.00 mmol) in ethanol (10 mL) was added dropwise to a solution of *tert*-butyl (4-*tert*-butyl-2-formyl-6-hydroximinomethylphenyl) sulfide (880 mg, 3.00 mmol) in ethanol (10 mL). After the reaction mixture was stirred overnight, a solution of $NaBH_4$ (500 mg, 13.20 mmol) in ethanol (10 mL) was added, and the mixture was stirred for a further 2 h. The ethanolic solution was then diluted with water (50 mL), and the excess reducing agent was destroyed by careful addition of 12 M HCl (final pH = 1). After 30 min of stirring, the pH of the solution was readjusted to pH ≈ 9 by dropwise addition of 2 M KOH solution, and the product was extracted three times with 100 mL of CH_2Cl_2. The organic phases were combined, and the solvent was removed in a vacuum. The resulting viscous oil was chromato-

(6) Niemann, A.; Bossek, U.; Wieghardt, K.; Butzlaff, C.; Trautwein, A. X.; Nuber, B. *Angew. Chem.* **1992**, *104*, 345−8; *Angew. Chem., Int. Ed. Engl.* **1992**, *31*, 311−4.
(7) Robin, M. B.; Day, P. *Adv. Inorg. Chem. Radiochem.* **1967**, *10*, 247−422.
(8) Creutz, C. *Prog. Inorg. Chem.* **1983**, *30*, 1−73.
(9) Allen, G. C.; Hush, N. S. *Prog. Inorg. Chem.* **1967**, *8*, 357−89.
(10) Hush, N. S. *Prog. Inorg. Chem.* **1967**, *8*, 391−444.
(11) Drüeke, S.; Chaudhuri, P.; Pohl, K.; Wieghardt, K.; Ding, X.-Q.; Bill, E.; Sawaryn, A.; Trautwein, A. X.; Winkler, H.; Gurman, S. J. *J. Chem. Soc., Chem. Commun.* **1989**, 59−62.
(12) Gamelin, D. R.; Bominaar, E. L.; Kirk, M. L.; Wieghardt, K.; Solomom, E. I. *J. Am. Chem. Soc.* **1996**, *118*, 8085−97.
(13) Beissel, T.; Glaser, T.; Kesting, F.; Wieghardt, K.; Nuber, B. *Inorg. Chem.* **1996**, *35*, 3936−47.
(14) Kersting, B.; Siebert, D. *Eur. J. Inorg. Chem.* **1999**, 189−93.
(15) Arnold, J. *Prog. Inorg. Chem.* **1995**, *43*, 353−417.
(16) Busch, D. H.; Jicha, D. C. *Inorg. Chem.* **1962**, *1*, 884−7.
(17) Konno, T.; Okamoto, K.-I.; Hidaka, J. *Acta Crystallogr.* **1993**, *C49*, 222−4.
(18) Liaw, W.-F.; Chen, C.-H.; Lee, C.-M.; Lin, G.-Y.; Ching, C.-Y.; Lee, G.-H.; Peng, S.-M. *J. Chem. Soc., Dalton Trans.* **1998**, 353−8.
(19) Beissel, T.; Birkelbach, F.; Bill, E.; Glaser, T.; Kesting, F.; Krebs, C.; Weyhermüller, T.; Wieghardt, K.; Butzlaff, C.; Trautwein, A. X. *J. Am. Chem. Soc.* **1996**, *118*, 12376−90.
(20) Glaser, T.; Kesting, F.; Beissel, T.; Bill, E.; Weyhermüller, T.; Meyer-Klaucke, W.; Wieghardt, K. *Inorg. Chem.* **1999**, *38*, 722−32.
(21) Glaser, T.; Beissel, T.; Bill, E.; Weyhermüller, T.; Schünemann, V.; Meyer-Klaucke, W.; Trautwein, A. X.; Wieghardt, K. *J. Am. Chem. Soc.* **1999**, *121*, 2193−208.
(22) Moreland, A. C.; Rauchfuss, T. B. *J. Am. Chem. Soc.* **1998**, *120*, 9376−7.
(23) Peters, J. W.; Lanzilotta, W. N.; Lemon, B. J.; Seefeldt, L. C. *Science* **1998**, *282*, 1853−8.
(24) Volbeda, A.; Charon, M.-H.; Piras, C.; Hatchikian, E. C.; Frey, M.; Fontecilla-Camps, J. C. *Nature* **1995**, *373*, 580−7.
(25) Nicolet, Y.; Piras, C.; Legrand, P.; Hatchikian, E. C.; Fontecilla-Camps, J. C. *Structure* **1999**, *7*, 13−23.
(26) Volbeda, A.; Garcin, E.; Piras, C.; de Lacey, A. L.; Fernandez, V. M.; Hatchikian, E. C.; Frey, M.; Fontecilla-Camps, J. C. *J. Am. Chem. Soc.* **1996**, *118*, 12989−96.
(27) Montet, Y.; Amara, P.; Volbeda, A.; Vernede, X.; Hatchikian, E. C.; Field, M. J.; Frey, M.; Fontecilla-Camps, J. C. *Nat. Struct. Biol.* **1997**, *4*, 523−6.
(28) Kersting, B.; Kolm, M. J.; Janiak, C. *Z. Anorg. Allg. Chem.* **1998**, *624*, 775−80.
(29) Kersting, B.; Siebert, D. *Inorg. Chem.* **1998**, *37*, 3820−8.
(30) N and N′ denote primary and secondary nitrogen atoms, respectively.
(31) Pilkington, N. H.; Robson, R. *Aust. J. Chem.* **1970**, *23*, 2225−36.
(32) Krüger, H.-J.; Holm, R. H. *Inorg. Chem.* **1987**, *26*, 3645−7.
(33) Krüger, H.-J.; Peng, G.; Holm, R. H. *Inorg. Chem.* **1991**, *30*, 734−42.
(34) Krüger, H.-J.; Holm, R. H. *J. Am. Chem. Soc.* **1990**, *112*, 2955−63.
(35) Musie, G.; Farmer, P. J.; Tuntulani, T.; Reibenspies, J. H.; Darensbourg, M. Y. *Inorg. Chem.* **1996**, *35*, 2176−83.
(36) Fleischer, E. B.; Gebala, A. E.; Levey, A.; Tasker, P. A. *J. Org. Chem.* **1971**, *36*, 3042−4.
(37) Kersting, B.; Steinfeld, G.; Hausmann, J. *Eur. J. Inorg. Chem.* **1999**, 179−87.
(38) The 200 MHz ^{1}H NMR data for $[Co_2(\mathbf{1})_3][ClO_4]_3$ in CD_3OD solution are given in ref 28. The 300 MHz ^{1}H NMR data for $[Co_2(\mathbf{1})_3][ClO_4]_3$ in DMSO-d_6 solution are as follows (for H-atom labeling see Chart 4 and Figure S3, Supporting Information): δ = 7.44 (s, 6H, Ar*H*), 5.65 (d, ^2J = 12.0 Hz, 6H, N*H*$^{h'}$), 5.44 (t, ^2J = ^3J = 12.0 Hz, 6H, N*H*^{h}), 3.86 (d, ^2J = 12.0 Hz, 6H, C*H*$^{e'}$), 3.64 (t, ^2J = ^3J = 12.0 Hz, 6H, C*H*^{e}), 1.29 (s, 27H, CH_3). ^{13}C NMR (75 MHz, DMSO-d_6): δ = 151.1, 139.1, 128.1, 125.9, 46.5, 35.0, 31.1.
(39) Wolsey, W. C. *J. Chem. Educ.* **1973**, *50*, A335.

graphed on SiO_2 (eluent 10% MeOH/CH_2Cl_2) to give 0.73 g (77%) of **2** as a white foam. ^{1}H NMR (CD_3OD): δ = 8.75 (s, 3H, C*H*NOH), 7.77 (d, ^4J = 2.0 Hz, 3H, Ar*H*), 7.44 (d, ^4J = 2.0 Hz, 3H, Ar*H*), 3.95 (s br, 6H, CH_2), 2.39 (s br, 6H, CH_2), 1.18 (s, 27H, CH_3), 1.10 (s, 27H, CH_3), 0.80 (s, 3H, CH_3). ^{13}C NMR (CD_3OD): δ = 153.8, 152.4 (CHN), 147.7, 140.4, 130.5, 129.7, 123.8, 57.9 (CH_2), 55.3 (CH_2), 50.6 (C_q), 39.7 (C_q), 36.2 (C_q), 32.4, 32.9, 22.8 (CH_3).

***N,N′,N″*-Tris[2-thio-3-aminomethyl-5-*tert*-butylbenzyl]-1,1,1-tris-(aminomethyl)ethane ($H_3$3·6HCl).** A solution of **2** (949 mg, 1.00 mmol) in THF (30 mL) was added dropwise to a solution of sodium (2.30 g, 0.10 mol) in liquid ammonia (100 mL). During addition the temperature was kept below −60 °C by cooling with a dry ice/2-propanol bath. After the deep blue reaction mixture was stirred for a further 3 h at −50 °C, solid ammonium chloride was added to destroy excess reducing equivalents. After the ammonia was allowed to evaporate at atmospheric pressure, the remaining THF was evaporated in a vacuum. The pale yellow residue was dissolved in 30 mL of water, and the pH of the solution was adjusted to pH ≈ 1 by addition of 1 M HCl. After 30 min of stirring, the resulting pale-yellow precipitate was collected by filtration and recrystallized from 1 M HCl to give 0.70 g (73%) of H_3**3**·6HCl as a white, microcrystalline solid. ^{1}H NMR (D_2O): δ = 7.30 (s, 6H, Ar*H*), 4.24 (s, 6H, CH_2), 4.10 (s, 6H, CH_2), 3.14 (s, 6H, CH_2), 1.19 (s, 3H, CH_3), 1.06 (s, 27H, CH_3). ^{13}C NMR (D_2O): δ = 151.7, 136.2, 133.3, 131.5, 130.2, 129.5, 53.0, 51.5, 43.4, 36.8, 34.6, 30.7, 18.2.

$[Co^{III}_2$(3)][ClO_4]$_3$ (4b). A solution of $CoCl_2$·$6H_2O$ (48 mg, 0.20 mmol) in methanol (2 mL) was added dropwise to a solution of H_3**3**·6HCl (96 mg, 0.10 mmol) in methanol (5 mL), and the resulting bluish-green solution was stirred for a further 10 min. A solution of NEt_3 (90 mg, 0.90 mmol) in methanol (1 mL) was then added to give a pale-red solution. Exposure of the reaction mixture to air initiated a color change to red-brown. After 2 h of stirring, the product was precipitated by addition of solid $LiClO_4$ (300 mg). The brown microcrystalline solid was isolated by filtration, washed with 1 mL of cold methanol and 5 mL of ether, and dried in air. Yield: 71 mg (60%). An analytical sample was obtained by recrystallization from a minimum amount of methanol. IR (KBr, cm^{-1}): $\tilde{\nu}$ = 1101 vs $\nu(ClO_4^-)$. ^{1}H NMR (300 MHz, CD_3-OD): δ = 7.58 (d, ^4J = 2.1 Hz, 3H, Ar*H*), 7.54 (d, ^4J = 2.1 Hz, 3H, Ar*H*), 4.31 (d, ^2J = 13.0 Hz, 3H, CH_2), 3.97 (d, ^2J = 13.0 Hz, 3H, CH_2), 3.89 (d, ^2J = 13.0 Hz, 3H, CH_2), 3.64 (d, ^2J = 13.0 Hz, 3H, CH_2), 3.48 (d, ^2J = 13.0 Hz, 3H, CH_2), 2.73 (d, ^2J = 13.0 Hz, 3H, CH_2) 1.33 (s, 27H, CH_3), 1.12 (s, 3H, CH_3). ^{1}H NMR (300 MHz, DMSO-d_6): δ = 7.54 (d, ^4J = 2.1 Hz, 3H, Ar*H*), 7.43 (d, ^4J = 2.1 Hz, 3H, Ar*H*), 6.54 (t, ^3J = 10.0 Hz, 3H, N*H*), 6.24 (d, ^2J = 12.0 Hz, 3H, NH*H*), 5.50 (t, ^2J = 12.0 Hz, 3H, N*H*H), 4.30 (t, ^2J = 12.0 Hz, 3H, CH_2), 3.87−3.97 (m, 9H, CH_2), 3.33 (obscured, 3H, CH_2), 2.52 (obscured, 3H, CH_2), 1.33 (s, 27H, CH_3), 1.00 (s, 3H, CH_3). ^{13}C NMR (75 MHz, CD_3OD): δ = 154.6, 140.9, 138.1, 130.4, 130.2, 126.3, 64.4, 61.2, 48.0, 42.3, 36.1, 31.4, 22.4. ^{13}C NMR (75 MHz, DMSO-d_6): δ = 151.1, 138.7, 136.5, 128.7, 127.8, 125.4, 62.1, 59.5, 45.7, 41.2, 34.7, 30.7, 21.7. Anal. Calcd for $C_{41}H_{63}N_6S_3Co_2Cl_3O_{12}$·$CH_3OH$: C, 42.59; H, 5.70; N, 7.10. Found: C, 42.43; H, 5.46; N, 6.88.

$[Co^{III}_2$(1)$_3$][Fe(CN)$_6$]·7CH_3OH·3H_2O (4c). To a solution of [Co_2-(**1**)$_3$][ClO_4]$_3$ (37 mg, 34.00 μmol) in methanol (25 mL) was added dropwise with stirring a solution of K_3[Fe(CN)$_6$] (11 mg, 34.00 μmol) in 2 mL of water. The solution was filtered and kept at room temperature for 2 days, during which time red crystals of **4c** formed. Yield: 32 mg (74%). Crystals of **4c** quickly lose the solvent molecules of crystallization upon storage in air at 298 K. IR (KBr, cm^{-1}): $\tilde{\nu}$ = 2106 s ν(CN). This compound was identified by an X-ray structure determination.

$[Ni^{III}Ni^{II}$(3)][BPh_4]$_2$ (5b). To a solution of H_3**3**·6HCl (96 mg, 0.10 mmol) in methanol (15 mL) was added a solution of $Ni(ClO_4)_2$·$6H_2O$ (73 mg, 0.20 mmol) in methanol (2 mL). The resulting purple solution was stirred for a further 10 min. Then a 0.90 mL portion of a 1.00 M NaOMe/MeOH solution (0.90 mmol) was added, resulting in a color change, from purple to pale-green. A solution of iodine (12.7 mg, 50.00 μmol) in methanol (2 mL) was added. To the resulting brown solution was added a solution of $NaBPh_4$ (151 mg, 0.44 mmol) in methanol (2 mL), and the resulting solution was kept at room temperature for 2 days, during which time 96 mg (63%) of **5b** precipitated as black crystals. IR (KBr, cm^{-1}): $\tilde{\nu}$ = 3330 s, 3252 s ν(NH) + $\nu(NH_2)$, 736 vs, 706 vs $\nu(BPh_4)$. Anal. Calcd for $C_{41}H_{63}N_6S_3Ni_2$·$B_2C_{48}H_{40}$·CH_3OH (M_r = 1524.06): C, 70.93; H, 7.08; N, 5.51. Found: C, 70.84; H, 6.84; N, 5.12.

$[Fe^{III}Fe^{II}$(3)][BPh_4]$_2$ (6b). To a solution of H_3**3**·6HCl (96 mg, 0.10 mmol) in methanol (15 mL) was added $FeCl_2$ (25 mg, 0.20 mmol) in methanol (2 mL). The resulting pale green solution was stirred for a further 10 min. A 0.90 mL portion of a 1.00 M solution of NaOMe in methanol (0.90 mmol) was added, and the flask was exposed to air. To the resulting dark blue solution was added a solution of $NaBPh_4$ (151 mg, 0.44 mmol) in methanol (2 mL), and the resulting solution was kept at room temperature for 2 days, during which time **6b** precipitated as black crystals. Yield: 62 mg (41%). IR (KBr, cm^{-1}): $\tilde{\nu}$ = 3300 s, 3228 s ν(NH) + $\nu(NH_2)$, 735 vs, 707 vs $\nu(BPh_4)$. Anal. Calcd for $C_{41}H_{63}N_6S_3Fe_2$·$B_2C_{48}H_{40}$·CH_3OH (M_r = 1518.37): C, 71.19; H, 7.10; N, 5.53. Found: C, 70.96; H, 7.04; N, 5.22.

$[Co^{III}Ni^{II}$(3)][BPh_4]$_2$ (7). A solution of $CoCl_2$·$6H_2O$ (48 mg, 0.20 mmol) in methanol (12 mL) was added dropwise to a solution of H_3**3**·6HCl (192 mg, 0.20 mmol) in methanol (10 mL), and the resulting bluish-green solution was stirred for a further 10 min. A solution of NEt_3 (182 mg, 1.80 mmol) in methanol (2 mL) was added, and the reaction mixture was exposed to air. The reaction mixture was stirred for a further 2 h in air to ensure complete oxidation of the intermediate complex [Co^{II}(**3**)]$^-$. An aqueous solution of $LiClO_4$ (1.0 M, 5 mL) was added and the pH of the solution adjusted to 1 by addition of 1 M HCl. The solution was filtered to remove a small quantity of a brown precipitate. Further water (20 mL) was added, and the resulting brown-black precipitate was isolated by filtration, washed with water, and dried in air. This material was dissolved in methanol (10 mL), and a solution of $Ni(ClO_4)_2$·$6H_2O$ (73 mg, 0.20 mmol) in methanol was added. Addition of a few drops of NEt_3 produced a color change to dark green. The solution was combined with a saturated aqueous solution of $LiClO_4$ (1.0 M, 5 mL) and 30 mL of water. The green solid, [$Co^{III}Ni^{II}$(**3**)]-[ClO_4]$_2$, was filtered, washed with water, and dried in air. Addition of a solution of $NaBPh_4$ in methanol (151 mg, 0.44 mmol) to the solution of [$Co^{III}Ni^{II}$(**3**)][ClO_4]$_2$ in methanol (10 mL) gives the air-stable tetraphenylborate salt [$Co^{III}Ni^{II}$(**3**)][BPh_4]$_2$. Yield: 74 mg (24%). This solid was recrystallized once from methanol. IR (KBr, cm^{-1}): $\tilde{\nu}$ = 3325 s, 3248 s ν(NH) + $\nu(NH_2)$, 736 vs, 707 vs $\nu(BPh_4)$. $C_{41}H_{63}N_6S_3$-CoNi·$B_2C_{48}H_{40}$·CH_3OH (M_r = 1524.30): C, 70.92; H, 7.08; N, 5.51. Found: C, 70.44; H, 6.92; N, 5.26.

$[Ni^{II}Co^{III}$(3)][BPh_4]$_2$ (8). To a degassed solution of H_3**3**·6HCl (96 mg, 0.10 mmol) in methanol (15 mL) was added a solution of Ni-$(ClO_4)_2$·$6H_2O$ (37 mg, 0.10 mmol) in methanol (2 mL). The resulting purple solution was stirred for a further 10 min. Then a 0.90 mL portion of a 1.00 M solution of NaOMe in methanol (0.90 mmol) was added, resulting in a color change, from purple to pale-green. To this solution was added dropwise with stirring a solution of $CoCl_2$·$6H_2O$ (24 mg, 0.10 mmol) in methanol (2 mL). After the solution was stirred for a further 30 min, the reaction mixture was exposed to air. The resulting dark green solution was stirred for a further 2 h. Addition of a solution of $NaBPh_4$ (151 mg, 0.44 mmol) in methanol (5 mL) initiated the precipitation of a green, microcrystalline precipitate of **8**. Yield: 42 mg (28%). This solid was recrystallized once from methanol. $C_{41}H_{63}N_6S_3$-CoNi·$B_2C_{48}H_{40}$·CH_3OH (M_r = 1524.30): C, 70.92; H, 7.08; N, 5.51. Found: C, 70.54; H, 6.83; N, 5.31.

X-ray Structure Determination. Diffraction-quality crystals of [Co_2-(**1**)$_3$][Fe(CN)$_6$]·7CH_3OH·3H_2O (**4c**, red-brown plates) were grown by the procedure described above. A red-brown crystal was removed from the mother liquor and immediately cooled to 183(2) K on a Bruker SMART diffractometer (three-circle goniometer with 1K CCD detector, Mo Kα radiation, graphite monochromator). Hemisphere data collection in ω at 0.3° scan width in three runs with 606, 435, and 230 frames (ϕ = 0°, 88°, and 180°) at a detector distance of 5 cm. A total of 32 396 reflections (1.5° < Θ < 25°) were collected of which 11 365 unique reflections (R_{int} = 0.072) were used. An empirical absorption correction using equivalent reflection was performed with the program SADABS.[40] The structure was solved with the program SHELXS-86[41] and refined

(40) Sheldrick, G. M. SADABS; University of Göttingen: Göttingen, Germany, 1997.

Table 1. Summary of Crystallographic Data for $[Co_2(\mathbf{1})_3][Fe(CN)_6]\cdot 7CH_3OH\cdot 3H_2O$

empirical formula	$C_{49}H_{91}N_{12}S_3O_{10}Co_2Fe$	fw	1278.23 g·mol^{-1}
		space group	*C*2/*c* (No. 15)
a	28.037(2) Å	*T*	−90(2) °C
b	17.861(1) Å	*λ*	0.710 73 Å (Mo Kα)
c	25.727(2) Å		
β	90.24(1)°	*μ*(Mo Kα)	0.887 mm^{-1}
V	12883.5(12) Å^3	R1,[a] wR2	0.0723, 0.1784
Z	8	$[I > 2\sigma(I)]$[b]	
ρ_{obsd}	1.318 g·cm^{-3}	R1, wR2 (all data)	0.1322, 0.2421

[a] $R1 = [\sum w(F_o - F_c)^2/\sum wF_o^2]^{1/2}$. [b] $wR2 = [\sum[w(F_o^2 - F_c^2)^2]/\sum w(F_o^2)^2]^{1/2}$, $w = 1/[\sigma^2(F_o^2) + (0.111P)^2 + 65.11P]$, where $P = (\max(F_o^2,0) + 2F_c^2)/3$.

using SHELXL-93[41] to R1 = 0.0723 for 6816 reflections with $I > 2\sigma(I)$. Further details of the data collection and refinement are summarized in Table 1.

Other Physical Measurements. ^{1}H NMR and ^{13}C{^{1}H} NMR spectra were recorded on a Bruker AC 200 spectrometer. The 2D COSY ^{1}H NMR spectra were recorded on a Varian Unity 300 spectrometer. CHN analyses were determined with a Perkin-Elmer elemental analyzer 240. IR spectra were recorded on a Bruker IFS25 spectrophotometer as KBr pellets. Absorption spectra were recorded in the range 300−1500 nm on a Jasco V-570 UV−vis−near-IR spectrophotometer. Cyclic voltammetry measurements were carried out at 25 °C with an EG&G Princeton Applied Research potentiostat/galvanostat model 263 A. The cell contained a Pt working electrode, a Pt wire auxiliary electrode, and a Ag wire as reference electrode. Concentrations of solutions were 0.1 M in supporting electrolyte ($Bu^n_4NPF_6$) and ca. 1×10^{-3} M in sample. Ferrocenium/ferrocene was used as internal standard. All potentials were converted to the SCE reference.[42] Coulometric experiments were performed with the use of a Pt-gauze electrode. EPR spectra were recorded by a conventional Varian X-band spectrometer with 100 kHz modulation.

^{57}Fe Mössbauer Spectroscopy. ^{57}Fe Mössbauer spectra were collected in constant acceleration modus with a triangular velocity profile and were digitalized in 1024 steps. ^{57}Co in a Rh matrix (AMERSHAM-Buchler) with an activity of about 60 MBq was used as *γ*-radiation source. The 14.41 keV *γ*-radiation was detected in transmission by a NaI(Tl) scintillation counter. The experimental spectra were iteratively approximated by least-squares procedures using the program package NORMOS.[43] Spectral parameters (δ, Γ, A, ΔE_Q) could each be fixed, opened, or correlated at will. Fits were aimed for with largely open parameters. The $\delta^{\alpha-Fe}$ scale of the isomer shift refers to the shift of α-iron ($\delta^{\alpha-Fe} = 0.11 \pm 0.01 + \delta^{Fe/Rh}$).[44] Complexes $[Fe^{II}_2(\mathbf{1})_3]Cl$ and $[Fe^{III}_2(\mathbf{1})_3][ClO_4]_3$ were prepared as described.[28] The mixed-valent iron complex $[Fe^{III}Fe^{II}(\mathbf{1})_3]^{2+}$ was prepared by sodium borohydride reduction of $[Fe^{III}_2(\mathbf{1})_3][ClO_4]_3$ and isolated as the tetraphenylborate salt $[Fe^{III}Fe^{II}(\mathbf{1})_3][BPh_4]_2$ (**6a**).[45] All samples were precooled under vacuum to collect the low-temperature spectra.

Results and Discussion

Ligand Synthesis. The nonadentate N_6S_3 ligand $H_3\mathbf{3}\cdot 6HCl$ could be obtained in good yields by the synthetic route depicted in Scheme 1. In the first step 3 equiv of *tert*-butyl (4-*tert*-butyl-2-formyl-6-hydroximinomethylphenyl) sulfide were condensed with 1 equiv of 1,1,1-tris(aminomethyl)ethane, followed by sodium borohydride reduction of the imine groups to give amine/oxime/thioether compound **2**. Cleavage of the ArylS−*t*-Bu bonds and reduction of the oxime functions was accomplished by reduction with an excess of sodium in liquid ammonia at −70 °C. The ligand was isolated as the hexahydrochloride salt $H_3\mathbf{3}\cdot 6HCl$, which is a pale-yellow solid that can be handled in air for short periods of time without any sign of oxidative decomposition. For long-term usage the compound was stored under an atmosphere of dry nitrogen.

Scheme 1. Preparation of $H_3\mathbf{3}\cdot 6HCl$

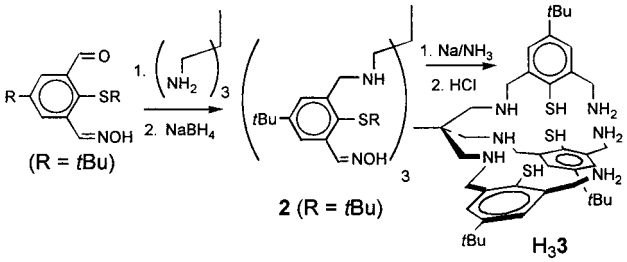

Syntheses of Metal Complexes. Homodinuclear Complexes. The complexes prepared and their labels are collected in Chart 3. The preparation of $[Co^{III}_2(\mathbf{1})_3][ClO_4]_3$ (**4a**) has been reported previously.[28] The tricationic complex $[Co^{III}_2(\mathbf{3})][ClO_4]_3$ (**4b**) was prepared in an analogous manner. Reaction of $H_3\mathbf{3}\cdot 6HCl$, $Co^{II}Cl_2\cdot 6H_2O$, and NEt_3 initially produces a pale-red solution containing the dicobalt(II) complex $[Co^{II}_2(\mathbf{3})]^+$, eq 1a, which rapidly oxidizes in the presence of air to give complex $[Co^{III}_2(\mathbf{3})]^{3+}$, eq 1b.

Chart 3. Synthesized Complexes and Their Labeling

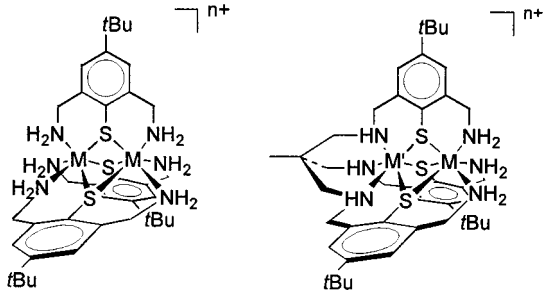

$[M_2(\mathbf{1})_3]^{n+}$

4a $[Co^{III}_2(\mathbf{1})_3][ClO_4]_3$

4c $[Co^{III}_2(\mathbf{1})_3][Fe^{III}(CN)_6]$

5a $[Ni^{III}Ni^{II}(\mathbf{1})_3][BPh_4]_2$

6a $[Fe^{III}Fe^{II}(\mathbf{1})_3][BPh_4]_2$

$[M'M(\mathbf{3})]^{n+}$

4b $[Co^{III}_2(\mathbf{3})][ClO_4]_3$

5b $[Ni^{III}Ni^{II}(\mathbf{3})][BPh_4]_2$

6b $[Fe^{III}Fe^{II}(\mathbf{3})][BPh_4]_2$

7 $[Co^{III}Ni^{II}(\mathbf{3})][BPh_4]_2$

8 $[Ni^{II}Co^{III}(\mathbf{3})][BPh_4]_2$

$$H_3\mathbf{3}\cdot 6HCl + 2CoCl_2\cdot 6H_2O \xrightarrow{NEt_3} [Co^{II}_2(\mathbf{3})]^+ \quad (1a)$$

$$[Co^{II}_2(\mathbf{3})]^+ \xrightarrow{O_2/LiClO_4} [Co^{III}_2(\mathbf{3})][ClO_4]_3 \quad (\mathbf{4b}) \quad (1b)$$

The air-stable perchlorate salt $[Co^{III}_2(\mathbf{3})][ClO_4]_3$ (**4b**) is a dark red microcrystalline solid, soluble in solvents like methanol, acetonitrile, dimethyl sulfoxide, and dimethylformamide. While the dinuclear nature of this complex is derived from its spectroscopic and electrochemical properties (vide infra), the structure of the $[Co^{III}_2(\mathbf{1})_3]^{3+}$ cation was confirmed by an X-ray

(41) Sheldrick, G. M. SHELXS-86; University of Göttingen: Göttingen, Germany, 1990. Sheldrick, G. M.; SHELXL-93; University of Göttingen: Göttingen, Germany, 1993.
(42) For formal potentials of the ferrocenium/ferrocene couple vs SCE, see: Connelly, N. G.; Geiger, W. E. *Chem. Rev.* **1996**, *96*, 877−910. Under our experimental conditions, the couple ferrocenium/ferrocene (Fc^+/Fc) is at $E_{1/2} = 0.45$ V (DMF) vs Ag.
(43) Brand, R. A. NORMOS, University of Duisburg, Germany, 1992.
(44) Stevens, J. G.; Gettys, W. L. In *Mössbauer isomer shift reference scales*; Shenoy, G. F., Wagner, F. E., Eds.; North-Holland Publ.: Amsterdam, New York, Oxford, 1978.
(45) The preparation of **6a** and the Mössbauer spectroscopic studies will be reported in more detail in a subsequent paper.

structure determination of $[Co^{III}_2(\mathbf{1})_3][Fe(CN)_6]\cdot 7CH_3OH\cdot H_2O$ (**4c**). This salt precipitates from an aqueous methanolic solution containing equimolar quantities of **4a** and $K_3Fe(CN)_6$.[46]

Similar to the preparation of monocationic $[Co^{II}_2(\mathbf{3})]^+$, complexes $[Ni^{II}_2(\mathbf{3})]^+$ and $[Fe^{II}_2(\mathbf{3})]^+$ are obtained by reaction of $Ni^{II}Cl_2\cdot 6H_2O$ or $Fe^{II}Cl_2$, $H_3\mathbf{3}\cdot 6HCl$, and NaOMe in a 2:1:9 stoichiometric ratio in methanol, eq 2a. These reactions demand a strict exclusion of air, otherwise the $[M^{II}_2(\mathbf{3})]^+$ complexes oxidize (by one electron) to give the mixed-valent $M^{III}M^{II}$ complexes $[M^{III}M^{II}(\mathbf{3})]^{2+}$, eq 2b. Oxidation may also be achieved with 0.5 equiv of iodine or by controlled potential electrolysis; the former reaction has been used in the preparation of $[Ni^{III}Ni^{II}(\mathbf{3})][BPh_4]_2\cdot MeOH$ (**5b**), eq 2c.

$$H_3\mathbf{3}\cdot 6HCl + 2MCl_2 \xrightarrow{NaOMe} [M^{II}_2(\mathbf{3})]^+ \quad (M = Ni \text{ or } Fe) \quad (2a)$$

$$[Fe^{II}_2(\mathbf{3})]^+ \xrightarrow{O_2/NaBPh_4} [Fe^{III}Fe^{II}(\mathbf{3})][BPh_4]_2 \quad (\mathbf{6b}) \quad (2b)$$

$$[Ni^{II}_2(\mathbf{3})]^+ \xrightarrow{I_2/NaBPh_4} [Ni^{III}Ni^{II}(\mathbf{3})][BPh_4]_2 \quad (\mathbf{5b}) \quad (2c)$$

The mixed-valent species can be further oxidized (by one electron) to give the fully oxidized $[M^{III}_2(\mathbf{3})]^{3+}$ species, eq 3. Interestingly, the dark-green dinickel(III) complex $[Ni^{III}_2(\mathbf{3})]^{3+}$ is much more stable ($\tau_{298°} \approx 2$ h) than the complex $[Ni^{III}_2(\mathbf{1})_3]^{3+}$ ($\tau_{298°} \approx {}^1/_4$ h),[29] presumably due to thermodynamic and kinetic stabilization by the nonadentate ligand $H_3\mathbf{3}$.

$$[M^{III}M^{II}(\mathbf{3})]^{2+} \xrightarrow{0.5I_2} [M^{III}_2(\mathbf{3})]^{3+} \quad (M = Ni \text{ or } Fe) \quad (3)$$

Heterodinuclear Complexes. Heterodinuclear complexes of Ni and Co were prepared by successive metalations of $H_3\mathbf{3}\cdot 6HCl$. The mononuclear Co^{II} complex $[Co^{II}(\mathbf{3})]^-$ (not isolated) was oxidized to inert $[Co^{III}(\mathbf{3})]$ prior to the addition of $Ni(ClO_4)_2\cdot 6H_2O$ to give the dark-green $Co^{III}Ni^{II}$ species $[Co^{III}Ni^{II}(\mathbf{3})]^{2+}$, eqs 4a,b.

$$H_3\mathbf{3}\cdot 6HCl + CoCl_2 \xrightarrow{NEt_3/O_2} [Co^{III}(\mathbf{3})] \quad (4a)$$

$$[Co^{III}(\mathbf{3})] + Ni(ClO_4)_2\cdot 6H_2O \xrightarrow{NaBPh_4} [Co^{III}Ni^{II}(\mathbf{3})][BPh_4]_2 \quad (\mathbf{7}) \quad (4b)$$

When the metal salts were added in the reverse order, it was also possible to obtain the linkage isomer, $[Ni^{II}Co^{III}(\mathbf{3})]^{2+}$, eqs 4c,d.

$$H_3\mathbf{3}\cdot 6HCl + Ni(ClO_4)_2\cdot 6H_2O \xrightarrow{NaOMe} [Ni^{II}(\mathbf{3})]^- \quad (4c)$$

$$[Ni^{II}(\mathbf{3})]^- + CoCl_2\cdot 6H_2O \xrightarrow{O_2/NaBPh_4} [Ni^{II}Co^{III}(\mathbf{3})][BPh_4]_2 \quad (\mathbf{8}) \quad (4d)$$

The formulation of $[Co^{III}Ni^{II}(\mathbf{3})]^{2+}$ and $[Ni^{II}Co^{III}(\mathbf{3})]^{2+}$ as discrete, heterodinuclear complexes is based on their characteristic UV−vis spectral and electrochemical properties, which are quite different from those of homodinuclear complexes $[Ni_2(\mathbf{3})]^{n+}$ and $[Co_2(\mathbf{3})]^{n+}$ (see below). Note that the properties of **7** and **8** are similar but not identical. Since the electronic absorption spectra and electrochemical properties of solutions of complexes **7** and **8** remain unchanged over periods of weeks, one can exclude inter- or intramolecular metal scrambling reactions.

(46) Cyanometalate anions are powerful reagents in isolating large cations of the same but opposite charge, see: Raymond, K. N.; Basolo, F. *Inorg. Chem.* **1966**, *5*, 949−50.

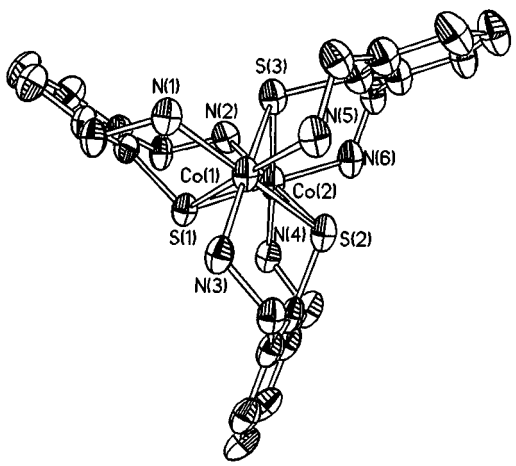

Figure 1. Perspective view of the molecular structure of the $[Co^{III}_2(\mathbf{1})_3]^{3+}$ trication in **4c** (50% probability thermal ellipsoids). Hydrogen atoms and *tert*-butyl groups are omitted for reasons of clarity.

Table 2. Selected Bond Lengths (Å) and Angles (deg) for $[Co_2(\mathbf{1})_3][Fe(CN)_6]\cdot 7CH_3OH\cdot 3H_2O$

Bond Lengths			
Co(1)−N(1)	1.989(5)	Co(2)−N(4)	1.985(6)
Co(1)−N(3)	1.993(5)	Co(2)−N(2)	1.994(5)
Co(1)−N(5)	1.998(5)	Co(2)−N(6)	1.992(5)
Co(1)−S(1)	2.261(2)	Co(2)−S(1)	2.247(2)
Co(1)−S(2)	2.275(2)	Co(2)−S(2)	2.271(2)
Co(1)−S(3)	2.257(2)	Co(2)−S(3)	2.248(2)
Co(1)···Co(2)	2.989(1)		

Bond Angles			
N(1)−Co(1)−N(3)	88.9(2)	N(2)−Co(2)−N(4)	90.0(2)
N(1)−Co(1)−N(5)	90.5(2)	N(2)−Co(2)−N(6)	90.4(2)
N(3)−Co(1)−N(5)	89.2(2)	N(4)−Co(2)−N(6)	90.0(2)
S(1)−Co(1)−S(2)	79.96(6)	S(1)−Co(2)−S(2)	80.34(6)
S(1)−Co(1)−S(3)	81.03(6)	S(1)−Co(2)−S(3)	81.53(7)
S(2)−Co(1)−S(3)	81.42(7)	S(3)−Co(2)−S(2)	81.69(7)
N(1)−Co(1)−S(1)	94.1(2)	N(2)−Co(2)−S(1)	94.7(2)
N(1)−Co(1)−S(2)	173.2(2)	N(2)−Co(2)−S(2)	172.8(2)
N(1)−Co(1)−S(3)	94.3(2)	N(2)−Co(2)−S(3)	92.5(2)
N(3)−Co(1)−S(1)	95.6(2)	N(4)−Co(2)−S(1)	93.9(2)
N(3)−Co(1)−S(2)	95.1(2)	N(4)−Co(2)−S(2)	95.5(2)
N(3)−Co(1)−S(3)	175.5(2)	N(4)−Co(2)−S(3)	174.9(2)
N(5)−Co(1)−S(1)	173.4(2)	N(6)−Co(2)−S(1)	173.6(2)
N(5)−Co(1)−S(2)	95.2(2)	N(6)−Co(2)−S(2)	94.2(2)
N(5)−Co(1)−S(3)	93.9(2)	N(6)−Co(2)−S(3)	94.4(2)

Since all homo- and heterodinuclear complexes were prepared by methods essentially identical with those used to prepare $[Co^{III}_2(\mathbf{3})]^{3+}$, all are assumed to be discrete, dinuclear species. This conclusion is, however, very strongly supported by both the spectroscopic and chemical properties of all. In particular, cyclic voltammetry measurements and EPR spectroscopic properties clearly define their dinuclear nature (vide infra).

Solid-State Structure of $[Co^{III}_2(\mathbf{1})_3][Fe^{III}(CN)_6]\cdot 7CH_3OH\cdot 3H_2O$ (4c). While mixed-valent $M^{III}M^{II}$ complexes of amine−thiolate ligand $H_1\mathbf{1}$ have been structurally characterized previously (M = Ni),[29] complex **4c** is the first example of a structurally characterized $[M_2(\mathbf{1})_3]^{n+}$ complex containing two trivalent metal ions. The crystal structure determination reveals the salt to consist of dinuclear trications $[Co^{III}_2(\mathbf{1})_3]^{3+}$, hexacyanoferrate anions, and methanol and water molecules of crystallization. The structure of the $[Fe^{III}(CN)_6]^{3-}$ anion is unexceptional and is not further considered. Figure 1 displays the structure of the dicobalt(III) complex. Table 2 summarizes selected bond distances and angles.

The trication is a confacial bioctahedron with two octahedral $N_3Co(SR)_3$ units bridged at the thiolate sulfur atoms (idealized C_{3h} symmetry). It is isostructural with the mixed-valent dication $[Ni^{III}Ni^{II}(\mathbf{1})_3]^{2+}$ in $[Ni_2(\mathbf{1})_3][BPh_4]_2$·MeOH (**5a**).[29] The average $Co^{III}-N$ and $Co^{III}-S$ distances at 1.992(5) and 2.260(2) Å, respectively, show no unusual features and compare well with those of other octahedral $N_3S_3Co^{III}$ complexes.[47,48] Both distances are shorter than the corresponding values in the d^7d^8 complex $[Ni^{III}Ni^{II}(\mathbf{1})_3]^{2+}$, and this in turn results in a shortening of the respective M···M distances from 3.064(1) Å in $[Ni^{III}Ni^{II}(\mathbf{1})_3]^{2+}$ to 2.989(1) Å in $[Co^{III}_2(\mathbf{1})_3]^{3+}$. On the basis of the relatively wide Co−S−Co angles (mean 82.8°), however, a direct attraction between the metal atoms is precluded.[1]

We note that we have also obtained preliminary X-ray crystallographic data for the mixed-valent diiron complex $[Fe^{III}Fe^{II}(\mathbf{1})_3][BPh_4]_2$ (**6a**). Although the structure determination is of low quality and not as good as desired for publication,[49] the present data can serve to confirm the atom connectivity of the $[Fe_2(\mathbf{1})_3]^{2+}$ cation. The preliminary structural data for complex $[Fe_2(\mathbf{1})_3]^{2+}$ reveals the dication to be isostructural with the Co^{III}_2 and $Ni^{III}Ni^{II}$ complexes $[Co^{III}_2(\mathbf{1})_3]^{3+}$ and $[Ni^{III}Ni^{II}(\mathbf{1})_3]^{2+}$, respectively. We also note a relatively short metal−metal distance at 2.78(2) Å (Fe−S−Fe = 70(1)°). It thus appears that $[M_2(\mathbf{1})_3]^{n+}$ type complexes (M = Fe, Co, and Ni)—irrespective of the choice of the metal and metal oxidation state—form an isostructural series of complexes featuring a central $N_3M(\mu_2\text{-}SR)_3MN_3$ core.

Although X-ray structural data for any of the $[M_2(\mathbf{3})]^{n+}$ species are currently not available, we assume that all exhibit a face-sharing bioctahedral $N_3M(\mu_2\text{-}SR)_3MN'_3$ core structure similar to that of the $[M_2(\mathbf{1})_3]^{n+}$ complexes (except for the atoms of the 1,1,1-tris(aminomethyl)ethane cap). The structure of the $[M_2(\mathbf{3})]^{n+}$ complexes may be derived from the solid-state structure of the $[Co_2(\mathbf{1})_3]^{3+}$ cation in **4c** by replacing one set of terminal amine protons (see Figure S1, Supporting Information) with the methylenic carbon atoms of a 1,1,1-tris(aminomethyl)-ethane moiety to afford two adjacent octahedral N'_3CoS_3 and N_3CoS_3 coordination sites. The assumption that the three secondary nitrogen atoms are facially bound to the same cobalt ion seems not unreasonable, given the fact that similar structures occur in some Co^{III} amine complexes, as for instance in the complexes $[Co^{III}(\text{sepulchrate})]^{3+}$, where sepulchrate denotes a hexadentate amine ligand derived from ethylenediamine and 1,1,1-tris(aminomethyl)ethane.[50] This is strongly supported by ^{1}H NMR spectroscopy.

Solution-State Structure of $[Co^{III}_2(3)][ClO_4]_3$ (4b). The ^{1}H NMR spectra of diamagnetic **4b** in CD_3OD (Figure S2, Supporting Information) or DMSO-d_6 solution (Figure 2) are fully consistent with the proposed structure shown in Chart 4. The spectra display the expected number of resonances; due to fast H/D exchange in methanol, NH protons were observed in DMSO-d_6 solution only.

Similar to the spectrum of the free ligand, the methyl and aromatic protons of **4b** in CD_3OD solution (Figure S2) appear as two singlets ($H^{a,b}$, see Chart 4 for atom labeling) and two doublets ($H^{c,d}$), respectively. Discrete spectral changes occur in the $\delta = 4.50-2.50$ ppm region, where the methylene protons $H^{e,f,g}$ resonate. While the free ligand displays three singlets, the complex gives rise to three well-resolved AB spin systems as indicated by three cross peaks in the off-diagonal area of the $^1H^1H$ COSY map. The AB spin system centered at $\delta = 3.11$ is assigned to methylene protons $H^{g,g'}$; the other two AB spin systems centered at $\delta = 3.81$ and 4.10 correspond to the remaining benzylic methylene protons. It is assumed that the AB system centered at 3.81 ppm is due to the benzylic protons of the CH_2NH_2 groups ($H^{e,e'}$), because this value is identical to that observed for $[Co^{III}_2(\mathbf{1})_3]^{3+}$.[38] Also consistent with the proposed structure for the $[Co^{III}_2(\mathbf{3})]^{3+}$ cation are the ^{13}C NMR data. As expected for a C_3-symmetric species, the spectrum displays 13 resonances for 13 inequivalent carbon atoms (6 for aromatic and 7 for aliphatic carbon atoms, see Experimental Section).

The three expected NH resonances were observed for the complex in DMSO-d_6 solution at $\delta = 6.54$ (t), 6.24 (d), and 5.50 (t) (Figure 2a). Assignment of these resonances to secondary (H^i) and primary amine hydrogen atoms ($H^{h,h'}$), respectively, is unambiguously achieved by $^1H^1H$ COSY spectroscopy (Figure 2b). In accordance with our assignment,

Chart 4. Proposed Structure for the $[Co_2(\mathbf{3})]^{3+}$ Trication with Atom Labeling (Top)[a]

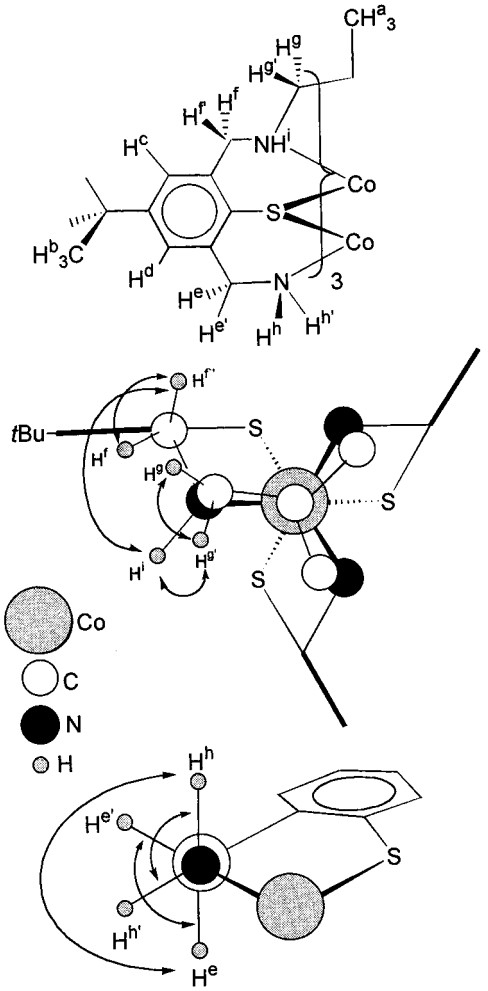

[a] Views along (middle) and perpendicular to (bottom) the C_3 axis emphasize different chemical environments for methylene and amine hydrogen atoms. Parts of the structure are omitted for reasons of clarity. Arrows represent geminal $^2J_{H,H}$ and vicinal $^3J_{H,H}$ couplings between methylene and amine hydrogen atoms. These correlations correspond to the cross peaks found in the respective COSY spectra.

(47) Okamoto, K.-I.; Aizawa, S.-I.; Konno, T.; Einaga, H.; Hidaka, J. *Bull. Chem. Soc. Jpn.* **1986**, *59*, 3859−64.
(48) Heeg, M. J.; Blinn, E. L.; Deutsch, E. *Inorg. Chem.* **1985**, *24*, 1118−20.
(49) Preliminary data of the crystal structure determination of $[Fe_2(\mathbf{1})_3][BPh_4]_2$·MeOH: monoclinic, space group $P2_1/n$, $a = 17.259(4)$ Å, $b = 39.938(5)$ Å, $c = 25.391(4)$ Å, $\beta = 109.72(8)°$, $V = 8238$ Å^3, $Z = 4$, μ(Mo Kα) = 0.48 mm^{-1}, $\rho = 1.328$ g·cm^{-3}, R1 = 0.0893 for 5190 $F_o > 4\sigma(F_o)$.
(50) Geue, R. J.; Hambley, T. W.; Harrowfield, J. M.; Sargeson, A. M.; Snow, M. R. *J. Am. Chem. Soc.* **1984**, *106*, 5478−88.

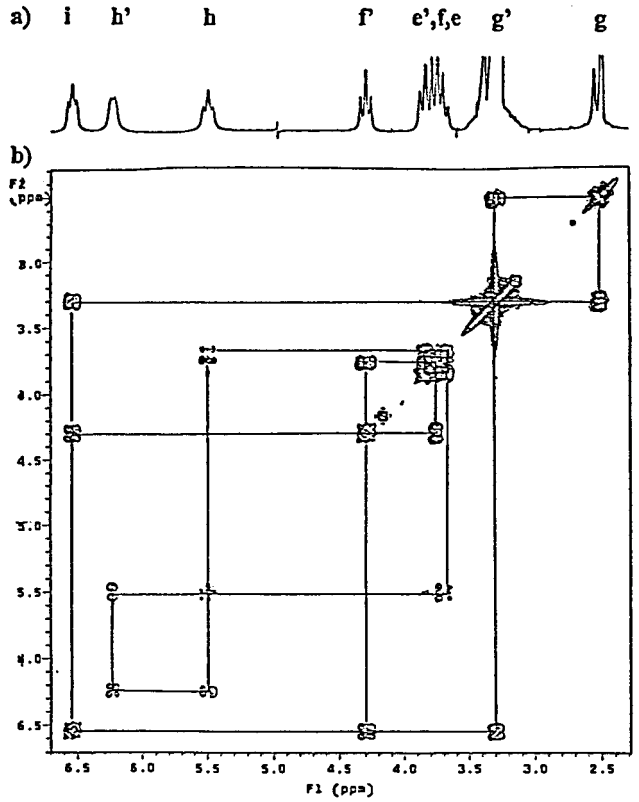

Figure 2. (a) One-dimensional ^{1}H NMR and (b) homonuclear 2D chemical shift correlation (COSY) spectra of $[Co^{III}_2(\mathbf{3})][ClO_4]_3$ in DMSO-d_6 solution (δ = 6.5−2.5 ppm region). The diagonal runs from the lower left to the upper right, reproducing the spectrum in part a. Lines between off-diagonal peaks and peaks on the diagonal indicate the respective homonuclear spin couplings. Resonances are assigned according to the structure shown in Chart 4. Resonances for $H^{g,g'}$ are obscured by resonances due to traces of H_2O in the deuterated solvent.

only the diagonal peaks at δ = 6.24 ($H^{h'}$) and δ = 5.50 (H^h) give rise to a cross peak ($|^2J_{h,h'}| \sim 13$ Hz). The hydrogen atom H^i, on the other hand, does not display geminal coupling with protons H^h or $H^{h'}$, but features cross peaks with methylene protons $H^{g'}$ and $H^{f'}$. Since the latter cross peaks reveal the AB spin systems centered at δ = 2.90 and 4.05 to be due to methylene hydrogen atoms $H^{g,g'}$ and $H^{f,f'}$, respectively, the remaining AB spin system centered at δ = 3.75 must be due to protons $H^{e,e'}$, which is in good agreement with our earlier assignment (vide supra).

Because one of the Co^{III} ions in the $[Co^{III}_2(\mathbf{3})]^{3+}$ trication is proposed to be facially coordinated by three CH_2NH_2 groups, there should exist some similarities between the NMR spectra of $[Co^{III}_2(\mathbf{1})_3]^{3+}$ and $[Co^{III}_2(\mathbf{3})]^{3+}$. In fact, a comparison of the one-dimensional ^{1}H NMR spectra of **4a** and **4b** in DMSO-d_6 solution reveals a similar pattern of resonances for the protons of the CH_2NH_2 moieties (Figures 2a and S3, Supporting Information). In **4a** the respective amine and methylene protons appear at δ = 5.65 (d, $H^{h'}$), 5.44 (t, H^h), 3.86 (d, $H^{e'}$), and 3.64 (t, H^e). The corresponding values for **4b** are at 6.24 (d, $H^{h'}$), 5.50 (t, H^h), 3.86 (d, $H^{e'}$), and 3.64 (t, H^e), with the resonances for the amine protons slightly shifted to lower field. For **4a**, the appearance of protons H^h and H^e as triplets is due to a geminal ($|^2J_{h,h'}|$, $|^2J_{e,e'}|$) and a vicinal coupling constant $|^3J_{h,e}|$ of similar magnitude of ≈12 Hz (Figure S3). In contrast, the appearance of resonances for protons $H^{h'}$ and $H^{e'}$ as doublets reveals significantly smaller vicinal coupling constants with adjacent protons (we estimate ^3J < 3 Hz). The different $^3J_{H,H}$ coupling constants indicate that the staggered conformation of

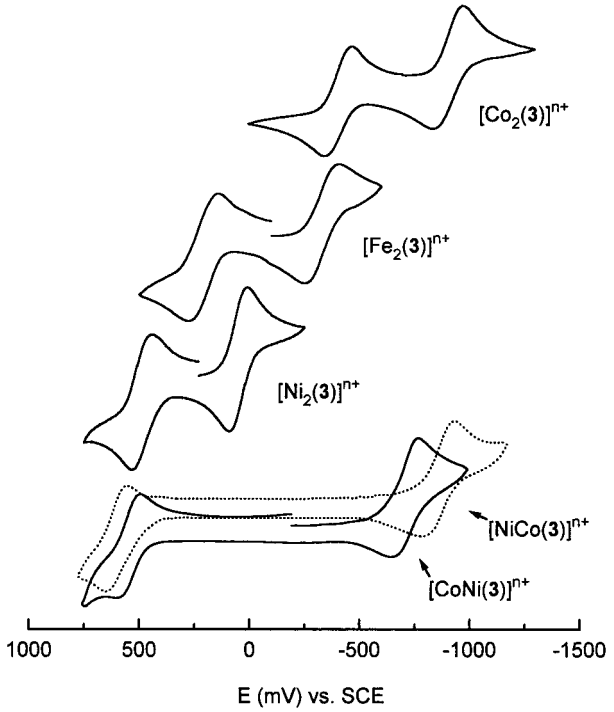

Figure 3. Cyclic voltammograms of $[Co^{III}_2(\mathbf{3})][ClO_4]_3$ (**4b**), $[Fe^{III}Fe^{II}(\mathbf{3})][BPh_4]_2$ (**6b**), $[Ni^{III}Ni^{II}(\mathbf{3})][BPh_4]_2$ (**5b**), $[Co^{III}Ni^{II}(\mathbf{3})][BPh_4]_2$ (**7**), and $[Ni^{II}Co^{III}(\mathbf{3})][BPh_4]_2$ (···, **8**) in DMF solution at 295 K. Experimental conditions: 0.1 M $[Bu^n_4N][PF_6]$, ca. 1×10^{-3} M sample concentration, Pt disk working electrode, Ag wire reference electrode, scan rate = 100 mV·s^{-1}.

the CH_2NH_2 groups found in the solid state (dihedral angles ϕ: 42° ($H^{e'}N-CH^{h'}$), 74° ($H^eN-CH^{h'}$, $H^{e'}N-CH^h$), and 170° (H^eN-CH^h)) is retained in the solution state. This is also in good agreement with the values for ^3J calculated by use of the Karplus equation. In this case $^3J_{H,H}(\phi = 170°) \gg {}^3J_{H,H}(\phi = 74°, \phi = 42°)$.[51]

The similar pattern of NMR resonances for the protons of the CH_2NH_2 groups suggests that one cobalt ion in $[Co^{III}_2(\mathbf{3})]^{3+}$ is facially bound by three CH_2NH_2 groups, similar to the coordination of Co^{III} in $[Co_2(\mathbf{1})_3]^{3+}$. The other Co ion is likewise considered to be facially coordinated by the three secondary nitrogen atoms of the tris(aminomethyl)ethane moiety. In our proposed structure, the dihedral angles $\phi(H^iN-CH^{g'})$ and $\phi(H^iN-CH^{f'})$ are estimated to be close to 0° and 180°, respectively. In this case, the Karplus equation predicts vicinal coupling constants of ≈12 Hz, which in turn would explain the triplet observed for H^i, and the absence of $^3J_{H,H}$ couplings to H^g, H^f.[52]

Electrochemical Properties. Homodinuclear Complexes. Examination of the complexes **4b**−**6b** via cyclic voltammetry in DMF solution showed two well-separated redox events in each case (see Figure 3). The presence of two consecutive electron-transfer steps in the CVs of complexes **4b**−**6b**, with potentials similar to those of the respective $[M_2(\mathbf{1})_3]^{n+}$ complexes **4a**−**6a**, further confirms their dinuclear nature. The potentials are referenced to the SCE and have been summarized in Table 3.

The two one-electron-reduction waves at $E^1_{1/2} = -0.40$ and at $E^2_{1/2} = -0.84$ V in the CV of **4b** (Figure 3) both exhibit the

(51) Hesse, M.; Meier, H.; Zeeh, B. *Spektroskopische Methoden in der organischen Chemie*, 5th ed.; Georg Thieme Verlag: Stuttgart, New York, 1995.

(52) Gray, A. G. In *Two-Dimensional NMR Spectroscopy*, 2nd ed.; Croasmun, W. R., Carlson, R. M. K., Eds.; VCH: Weinheim, 1994.

Table 3. Electrochemical Data, E (V), for $[M_2(\mathbf{1})_3]^{n+}$ and $[M_2(\mathbf{3})]^{n+}$ Complexes[a]

compound	$E^1_{1/2}$ ($M^{III,III}/M^{III,II}$)[b]	$E^2_{1/2}$ ($M^{III,II}/M^{II,II}$)[b]	$\Delta E^x_{1/2}$[c]	K_c[d]
Homodinuclear Complexes				
$[Co_2(\mathbf{1})_3]^{n+}$, **4a**	−0.47 (132)	−0.85 (127)	0.38	2.6×10^6
$[Co_2(\mathbf{3})]^{n+}$, **4b**	−0.40 (119)	−0.84 (136)	0.44	2.8×10^7
$[Ni_2(\mathbf{1})_3]^{n+}$, **5a**[e]	+0.46 (84)	+0.02 (73)	0.44	2.8×10^7
$[Ni_2(\mathbf{3})]^{n+}$, **5b**	+0.49 (87)	+0.05 (82)	0.44	2.8×10^7
$[Fe_2(\mathbf{1})_3]^{n+}$, **6a**	+0.18 (134)	−0.35 (163)	0.53	9.2×10^8
$[Fe_2(\mathbf{3})]^{n+}$, **6b**	+0.21 (135)	−0.33 (154)	0.54	1.4×10^9
Heterodinuclear Complexes				
$[CoNi(\mathbf{3})]^{n+}$, **7**	+0.55 (96)[f]	−0.71 (119)[g]	1.26	
$[NiCo(\mathbf{3})]^{n+}$, **8**	+0.60 (97)[f]	−0.86 (133)[g]	1.46	

[a] Data recorded in DMF solution. Conditions: Pt disk working electrode, Pt wire auxiliary electrode, Ag wire reference electrode, scan rate 100 mV·s^{-1}. Solutions were ca. 1×10^{-3} M in sample and 0.1 M in $N^nBu_4PF_6$. All potentials are referenced to the SCE. [b] $E^x_{1/2} = (E^{ox}_p + E^{red}_p)/2$ for reversible one-electron-transfer processes; values in parentheses represent peak-to-peak separations ($\Delta E_p = |E^{ox}_p - E^{red}_p|$). [c] $\Delta E^x_{1/2} = |E^1_{1/2} - E^2_{1/2}|$. [d] $K_c = \exp(38.94\Delta E^x_{1/2})$, at $T = 298$ K. [e] Values taken from ref 29. [f] Values represent $Ni^{III/II}$ potentials. [g] Values represent $Co^{III/II}$ potentials.

characteristics of quasi-reversible charge-transfer processes. At all scan rates (50−500 mV·s^{-1}), the ratio $i_{pc}/i_{pa} \approx 1$, $i_p/\nu^{1/2}$ is independent of scan rate, and anodic to cathodic peak-to-peak separations $\Delta E^1_p = 119$ mV and $\Delta E^2_p = 136$ mV (at 100 mV·s^{-1}) increase slightly with scan rate. Reduction of $[Co^{III}_2(\mathbf{3})]^{3+}$ at a constant potential of −0.60 V required 0.97 e$^-$/complex, and reduction at −1.0 V consumed 1.89 e$^-$/complex. Since the amine−thiolate ligand $\mathbf{3}^{3-}$ in $[Co^{III}_2(\mathbf{3})]^{3+}$ is unlikely to undergo ligand-centered redox reactions, it is concluded that both reduction waves correspond to metal-centered redox reactions, eqs 5a,b (M = Co), with successive formation of the mixed-valent $Co^{III}Co^{II}$ and fully reduced Co^{II}_2 forms.

$$[M^{III}M^{III}(\mathbf{3})]^{3+} + e^- \rightarrow [M^{III}M^{II}(\mathbf{3})]^{2+} \qquad E^1_{1/2} \quad (5a)$$

$$[M^{III}M^{II}(\mathbf{3})]^{2+} + e^- \rightarrow [M^{II}M^{II}(\mathbf{3})]^{+} \qquad E^2_{1/2} \quad (5b)$$

Electrochemically generated solutions of $[Co^{III}Co^{II}(\mathbf{3})]^{2+}$ and $[Co^{II}_2(\mathbf{3})]^+$ exhibit characteristic electronic absorption spectra, which remain unchanged for days under anaerobic conditions. These species could also be prepared by sodium borohydride reduction of $[Co^{III}_2(\mathbf{3})]^{3+}$, as indicated by UV−vis spectroscopy. The $Co^{II}Co^{II}$ and $Co^{III}Co^{II}$ complexes, when exposed to air, readily underwent reoxidation to the red-brown Co^{III}_2 complex. The respective electron-transfer processes are thus also chemically reversible.

The CVs of the nickel and iron complexes **5b** and **6b**, respectively, are shown in Figure 3. There are also two consecutive redox waves, however, at more anodic potentials at $E^1_{1/2} = +0.49$ and at $E^2_{1/2} = +0.05$ V (**5b**) and at $E^1_{1/2} = +0.21$ and at $E^2_{1/2} = -0.33$ V (**6b**) vs SCE, respectively. Here, the processes at $E^1_{1/2}$ correspond to a one-electron oxidation to give the fully oxidized $[M^{III}_2(\mathbf{3})]^{3+}$ species, whereas a one-electron reduction at $E^2_{1/2}$ produces the fully reduced $[M^{II}_2(\mathbf{3})]^+$ species. The one-electron nature of all processes was confirmed by controlled potential coulometry.

All mixed-valent complexes are very stable to disproportionation, as quantified by the comproportionation constant K_c defined for the equilibrium shown in eq 6. Comproportionation constants for **4a**−**6b** calculated from eq 7 have been placed in Table 3.

For the cobalt and nickel complexes, the difference $\Delta E^x_{1/2} = |E^1_{1/2} - E^2_{1/2}|$ appears to be nearly invariably ∼0.38−0.44 V

$$[M^{II}_2(\mathbf{3})]^+ + [M^{III}_2(\mathbf{3})]^{3+} = 2[M^{III}M^{II}(\mathbf{3})]^{2+} \qquad K_c \quad (6)$$

$$\Delta E = |E^1_{1/2} - E^2_{1/2}| = \frac{RT}{nF} \ln K_c \qquad (7)$$

$$\Delta G_c = \frac{1}{2} RT \ln(K_c/4) \qquad (8)$$

irrespective of the choice of the ligand and metal. Similar values have been reported for several homo- and heterotrinuclear amine−thiolate complexes of the type [LMMML], [LMM^{1}ML], and [LMMM^{1}L] all of which contain a central $N_3M(\mu_2\text{-}SR)_3M(\mu_2\text{-}SR)_3MN_3$ core (M, M^1 = Co, Ni, see Chart 5 for the

Chart 5

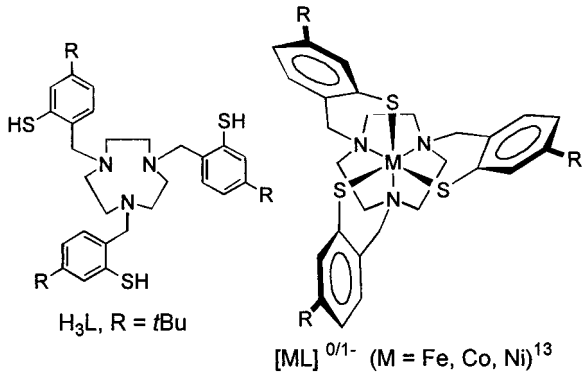

structure of the ligand H_3L).[19] It is thus surprising that the Fe^{III}-Fe^{II} complexes are approximately 2 orders of magnitude more stable to disproportionation than the nickel complexes, with K_c (**6a**,**b**) ∼30−50 × K_c (**5a**,**b**). The difference in K_c amounts to a relative stabilization of ∼4−5 kJ·mol^{-1} in the free energy of comproportionation, ΔG_c (ΔG_c = 23.9 kJ·mol^{-1} (**6a**), 24.4 kJ·mol^{-1} (**6b**), and 19.6 kJ·mol^{-1} (**5a**,**b**)).

For mixed-valent $Ru^{II}Ru^{III}$ complexes four factors have been recognized to contribute to the magnitude of ΔG_c, the free energy of comproportionation per mole of mixed-valence dimer, eq 9,[8,53]

$$\Delta G_c = \Delta G_R + \Delta G_e + \Delta G_E + \Delta G_S \qquad (9)$$

where ΔG_R is the free energy of resonance exchange, while ΔG_e, ΔG_E, and ΔG_S, are related, respectively, to an entropic factor ($^1/_2$ RT ln($^1/_4$)), an electrostatic factor arising from the repulsion of the two similarly charged metal centers, and a synergistic factor due to stabilization of M^{II} by M^{III} or vice versa. The electrostatic effects depend on the detailed structures (shapes, charges) and on the solvent.

It is likely that several such factors also contribute to ΔG_c for the complexes investigated in this study, including stabilization by resonance exchange,

$$\Delta G_c = \Delta G_R + \Sigma\Delta G_i \qquad (10)$$

Assuming that $\Delta G_R \sim 0$ for the nickel complexes (localized valencies, no resonance stabilization), the value of ∼ 20 kJ·mol^{-1} for ΔG_c (**5a**,**b**) can be considered to be entirely due to nonexchange contributions, $\Sigma\Delta G_i$. The similar value in ΔG_c determined for the cobalt complexes would be consistent with this in view. It is likely that the same factors should contribute with ∼20 kJ·mol^{-1} to the stability of the mixed-valent iron complexes. The difference in ΔG_c of the nickel and cobalt

(53) Sutton, J. E.; Taube, H. *Inorg. Chem.* **1981**, *20*, 3125−34.

complexes and the iron complexes ($\Delta(\Delta G_c) \sim 4-5$ kJ·mol^{-1}) may then be considered to be due to additional stabilization by resonance exchange ΔG_R. We realize that other factors may contribute to the stabilization (destabilization) of **6a**,**b** as well; however, the stabilization by resonance exchange must be taken into account. This is also supported by the results of preliminary ^{57}Fe Mössbauer spectroscopic studies presented below for **6a**.

Heterodinuclear Complexes. Similar to homodinuclear complexes **4a**−**6b** both heterodinuclear complexes also give rise to two one-electron waves in their cyclic voltammograms. The CVs differ, however, dramatically from those of the homodinuclear complexes (see Figure 3). That of **7** displays a reduction wave at $E^2_{1/2} = -0.71$ V which, by comparison with that of **4b**, should correspond to reduction of the Co^{III} ion (eq 11b, M = Co, M′ = Ni). The other wave at $E^1_{1/2} = +0.55$ V is then assigned to oxidation of the Ni^{II} ion to form the $Co^{III}Ni^{III}$ species $[Co^{III}Ni^{III}(\mathbf{3})]^{3+}$ (eq 11a, M = Co, M′ = Ni). The corresponding values in the linkage isomer **8** are shifted to more cathodic and anodic potentials at $E^2_{1/2} = -0.86$ and at $E^1_{1/2} = +0.60$ V (eqs 11c,d; M = Ni, M′ = Co). Note that in both cases the ΔE_p value for the $Ni^{III/II}$ couple is smaller at ∼96 mV than that of the $Co^{III/II}$ couple with $\Delta E_p \sim 125$ mV. Similar ΔE_p values were observed for the respective couples in the homodinuclear complexes, providing further support for the assignments (vide supra).

$$[M^{III}M'^{III}(\mathbf{3})]^{3+} + e^- \rightarrow [M^{III}M'^{II}(\mathbf{3})]^{2+} \quad ([M^{II}M'^{III}(\mathbf{3})]^{2+}) \qquad E^1_{1/2} \quad (11a(c))$$

$$[M^{III}M'^{II}(\mathbf{3})]^{2+} \quad ([M^{II}M'^{III}(\mathbf{3})]^{2+}) + e^- \rightarrow [M^{II}M'^{II}(\mathbf{3})]^{+} \qquad E^2_{1/2} \quad (11b(d))$$

The electrochemical properties of the linkage isomers are similar but not identical. There are clearly discernible anodic shifts in $Co^{III/II}$ and $Ni^{III/II}$ potentials upon changing the donor set from N_3S_3 to N'_3S_3 for a given metal ion.[30] The $Co^{III/II}$ potential, for example, shifts from −0.86 V in **8** (N_3S_3 donor set) to −0.71 V in **7** (N'_3S_3 donor set). The potential for the $Ni^{III/II}$ couple is likewise shifted to more anodic potentials upon changing the donor set from N_3S_3 to N'_3S_3; however, the effects are less dramatic. The observed anodic shifts in potentials for the N'_3S_3M fragments can be attributed to the weaker ligand field strength of the N'_3S_3 donor set relative to that of N_3S_3.[54]

Comparison of Electrochemical Data. Several studies have appeared in the literature in determining the factors that lead to the stabilization of Ni^{III},[32−35,55] because this oxidation state has been implicated with the function of [NiFe]-hydrogenase from *D. gigas*.[56−58] It is thus of significance that (a) the nickel complexes in this study may be reversibly oxidized to species containing Ni^{III}, (b) the corresponding $Ni^{III/II}$ potentials occur at relatively low values, and (c) the potentials span a range of ca. 0.60 V (from +0.60 V in **8** to +0.02 V in **5a**), despite the fact that the overall coordination of nickel is always N_3S_3. In the following we will show that the leading factors that influence the potential of the $Ni^{III/II}$ couple in dinuclear $N_3Ni(\mu_2\text{-}SR)_3M'N_3$ assemblies are (i) S-metalation and (ii) the oxidation state of the adjacent metal atom M′ (neglecting the small influence of N or N′ coordination).

Darensbourg et al.[59] have examined the effects of sulfur modification (S-alkylation, H-bonding, metalation, and oxygenation) on the redox properties of nickel in nickel amine−thiolate complexes of the type N_2S_2Ni. These modifications resulted exclusively in considerable anodic shifts in $Ni^{II/I}$ as well as $Ni^{III/II}$ potentials, and the authors come to the conclusion that *μ_2-bridging thiolates are metalated versions of thioethers*. If the $M^{III/II}$ redox potentials (E_{mid} values were taken, $E_{mid} = (E^1_{1/2} + E^2_{1/2})/2$) of homodinuclear complexes **4a** (−0.66 V), **6a** (−0.085 V), and **5a** (+0.24 V) are compared with those of their mononuclear analogues, [ML] (see Chart 5 for structures of complexes [ML]; $E_{1/2}$ ($M^{III/II}$) = −0.63 V for $[FeL]^{0/-}$, −0.24 V for $[NiL]^{0/-}$),[13,60] the effect of S-metalation on the $M^{III/II}$ potentials is also seen in the compounds examined in this study. Here, it causes an anodic shift of ∼ +0.5 V in the $M^{III/II}$ potentials, irrespective of the choice of the metal. The effect is, however, less dramatic than in the N_2S_2Ni complexes, where it produces anodic shifts of 1−1.5 V.

Now that more electrochemical data are available, in particular for heterodinuclear complexes **7** and **8**, it is also possible to study the influence of the oxidation state of M′ on $E_{1/2}$ ($Ni^{III/II}$). Consider, for example, complexes **7** and **8**, where the oxidation state of the adjacent metal atom is +3 ($Co^{III}Ni^{II}$). Here the $Ni^{III/II}$ potentials occur at a relatively high anodic potential of ca. +0.55 to +0.66 V vs SCE. These values should be compared with the $Ni^{III/II}$ couple at $E^2_{1/2} = +0.02$ V for **5a**, where the oxidation state of the adjacent metal atom is now +2 (Ni^{II}-Ni^{II}). Thus, decreasing the formal oxidation state of M′ results in cathodic shifts in $Ni^{III/II}$ potentials. It is thus likely that the Ni^{III} state can be similarly accommodated—and stabilized—in the $(RS)_2Ni(\mu_2\text{-}SR)_2(X)Fe(CO)_2CN$ active site in [NiFe]-hydrogenase from *D. gigas*, because of the presence of the Fe^{II} site.

UV/Vis Spectroscopy. The $[M_2(\mathbf{3})]^{n+}$ species are readily identified by their electronic absorption spectra. In Figures S4−S6 (Supporting Information) are displayed the electronic absorption spectra of the $[Ni_2(\mathbf{3})]^{n+}$, $[Co_2(\mathbf{3})]^{n+}$ and $[Fe_2(\mathbf{3})]^{n+}$species ($n = 1-3$) in DMF solution. Electronic absorption spectral data for the complexes are collected in Table 4.

In general, the electronic absorption spectra of the $M^{III}M^{II}$ and $M^{III}{}_2$ complexes are dominated by several intense features which can be ascribed to either $\pi \rightarrow \pi^*$ transitions of the ligands (λ in the range 300−400 nm) or to ligand-to-metal charge-transfer transitions ($\lambda > 400$ nm). The less intense bands in the fully reduced $M^{II}{}_2$ complexes, on the other hand, are thought to be due to ligand field (d−d) transitions. The weak absorption band at $\lambda_{max} = 1110$ nm in the spectrum of $[Co^{II}{}_2(\mathbf{3})]^+$, for example, is tentatively assigned to the $^4T_{1g} \rightarrow {}^4T_{2g}$ transition of an octahedral $N_3S_3Co^{II}$ chromophore. For $[Ni^{II}{}_2(\mathbf{3})]^+$, weak absorption bands occur at $\lambda_{max} = 606$ nm and at 944 and 1035 nm. They correspond to the $^3A_{2g} \rightarrow {}^3T_{1g}$ and $^3A_{2g} \rightarrow {}^3T_{2g}$ (splitting due to lower symmetry) transitions, respectively, of an octahedral Ni^{II} ion. Relative to the absorption bands of $[Ni_2(\mathbf{1})_3]^+$, those of $[Ni_2(\mathbf{3})]^+$ are shifted to lower energies, indicative of a slightly weaker ligand field strength of $H_3\mathbf{3}$. The weaker ligand field of $H_3\mathbf{3}$ relative to $H_1\mathbf{1}$ can be attributed to partial conversion of primary into secondary amine nitrogen atoms.[54]

(54) Wagner, F.; Barefield, E. K. *Inorg. Chem.* **1976**, *15*, 408−17.
(55) Fox, S.; Wang, Y.; Silver, A.; Millar, M. *J. Am. Chem. Soc.* **1990**, *112*, 3218−20.
(56) Cammack, R.; Fernandez, V. M.; Schneider, K. In *The Bioinorganic Chemistry of Nickel*; Lancaster, J. R., Jr., Ed.; VCH Publishers: New York, 1988; Chapter 4.
(57) Halcrow, M. A.; Christou, G. *Chem. Rev.* **1994**, *94*, 2421−81.
(58) Halcrow, M. A. *Angew. Chem.* **1995**, *107*, 1307−10; *Angew. Chem., Int. Ed. Engl.* **1995**, *34*, 1193−7.
(59) Farmer, P. J.; Reibenspies, J. H.; Lindahl, P. A.; Darensbourg, M. Y. *J. Am. Chem. Soc.* **1993**, *115*, 4665−74.
(60) The cobalt complex $[Co^{III}L]$ cannot be reduced reversibly to the $[Co^{II}L]^-$ species, see ref 13. Throughout the text, redox potentials have been quoted according to the reference standard and units, respectively, employed by the original authors; these data were converted to a common scale (SCE), however, to aid comparison (see ref 42).

Table 4. UV−Vis Spectral Properties, λ_{max} (nm) (ϵ (M^{-1} cm^{-1})), of Complexes **4b**−**8**[a]

Complex **4b**	
$[Co^{II}_2(\mathbf{3})]^{+}$	352 (2239), 454 sh (730), 536 sh (278), 1110 (24)
$[Co^{III}Co^{II}(\mathbf{3})]^{2+}$	367 (6475), 462 sh (1630), 581 sh (1010)
$[Co^{III}_2(\mathbf{3})]^{3+}$	370 (10 192), 422 sh (6769), 478 sh (2631), 579 sh (967)
Complexes **5a**,**b**	
$[Ni^{II}_2(\mathbf{1})_3]^{+}$ [b]	397 (2763), 593 (177), 922 (113), 1024 (103)
$[Ni^{II}_2(\mathbf{3})]^{+}$	392 (3123), 606 (114), 944 (94), 1035 (84)
$[Ni^{III}Ni^{II}(\mathbf{1})_3]^{2+}$ [b]	391 (7144), 473 (6753), 580 sh (4022)
$[Ni^{III}Ni^{II}(\mathbf{3})]^{2+}$	390 (7764), 462 (6293), 580 sh (3570), 851 (642)
$[Ni^{III}_2(\mathbf{1})_3]^{3+}$ [b]	614 (6959)
$[Ni^{III}_2(\mathbf{3})]^{3+}$	393 (10 573), 465 (10 085), 619 (6620), 801 (1470)
Complexes **6a**,**b**	
$[Fe^{II}_2(\mathbf{1})_3]^{+}$	308 (4612), 532 (410), 713 (125)
$[Fe^{II}_2(\mathbf{3})]^{+}$	303 (8270), 549 (637), 750 (173)
$[Fe^{III}Fe^{II}(\mathbf{1})_3]^{2+}$	319 (9350), 554 (1650), 751 sh (416), 1406 (450)
$[Fe^{III}Fe^{II}(\mathbf{3})]^{2+}$	350 (13 027), 563 (1783), 732 (488), 1280 (532)
$[Fe^{III}_2(\mathbf{1})_3]^{3+}$	312 (19 612), 416 sh (4101), 506 sh (1901), 700 (125)
$[Fe^{III}_2(\mathbf{3})]^{3+}$	345 (10 977), 402 sh (7736), 537 sh (1428), 752 (140)
Complexes **7**, **8**	
$[Co^{III}Ni^{II}(\mathbf{3})]^{2+}$	463 (2310), 615 (624), 899 (75)
$[Ni^{II}Co^{III}(\mathbf{3})]^{2+}$	465 (2139), 604 (572), 900 sh (65)

[a] Spectra were recorded at 298 K, sh = shoulder. MeOH as solvent for $[M^{II}_2(\mathbf{1})_3]^{+}$, $[M^{II}_2(\mathbf{3})]^{+}$ (M = Fe, Co), concentrations were 3.0×10^{-4} M; DMF as solvent for all other species with a concentration of 4.0×10^{-4} M. [b] Values taken from ref 29.

Before we discuss the electronic absorption spectra of the mixed-valent species, we shall briefly recall the results of the crystal structure determination of the $[Ni^{III}Ni^{II}(\mathbf{1})_3]^{2+}$ dication,[29] which characterized this complex to be class I in Robin and Day's classification of mixed-valence species (with distinct localized $N_3S_3Ni^{II}$ and $N_3S_3Ni^{III}$ sites). The interpretation of its electronic absorption spectrum was, however, hampered by the instability of the fully oxidized $Ni^{III}Ni^{III}$ form, $[Ni^{III}_2(\mathbf{1})_3]^{3+}$. The absorption spectrum of the $Ni^{III}Ni^{III}$ species, by comparison with that of the mixed-valent $Ni^{III}Ni^{II}$ form, could have helped in an assignment of the respective bands as ligand-to-metal (CT) or metal-to-metal (IT) charge-transfer transitions. It is therefore gratifying to note that the enhanced stability of the $Ni^{III}Ni^{III}$ complex $[Ni^{III}_2(\mathbf{3})]^{3+}$ now enables us to observe the electronic absorption spectral data of a $N_3Ni^{III}(\mu_2\text{-}SR)_3Ni^{III}N_3$ chromophore without interference from bands arising from its decomposition products. The spectra reveal complexes $[Ni^{III}_2(\mathbf{3})]^{3+}$ and $[Ni^{III}Ni^{II}(\mathbf{3})]^{2+}$ to exhibit three intense bands at very similar positions. Apparently, there are no new features in the spectrum of the mixed-valence complex, and consequently, all can be assigned as predominantly ligand-to-metal charge-transfer transitions. The three bands in the spectrum of $[Ni^{III}Ni^{II}(\mathbf{1})_3]^{2+}$ are likewise considered to be due to CT transitions, because they occur at positions similar to those of $[Ni^{III}Ni^{II}(\mathbf{3})]^{2+}$. It is assumed that the localized oxidation state distribution in both compounds is primarily due to differences in metal−ligand distances in the constituent $N_3S_3Ni^{III}$ (low-spin d^7 electronic configuration, Jahn−Teller distortion) and $N_3S_3Ni^{II}$ sites. Similar conclusions can be drawn for the mixed-valent $Co^{III}Co^{II}$ complex for which localized valencies Co^{III} (low-spin d^6) and Co^{II} (d^7) are considered.

Figure S7 (Supporting Information) shows the electronic absorption spectra of the mixed-valent iron complex $[Fe_2(\mathbf{1})_3]^{n+}$ (**6a**) in DMF solution. The spectrum differs from that of the mixed-valent nickel (or cobalt) complexes in that it shows, besides the CT bands at 554 and 751 nm, an additional intense band in the near-infrared region at 1406 nm ($\epsilon = 450$ M^{-1} cm^{-1}; fwhm (full width at half-maximum) = 2107 cm^{-1}). Surprisingly,

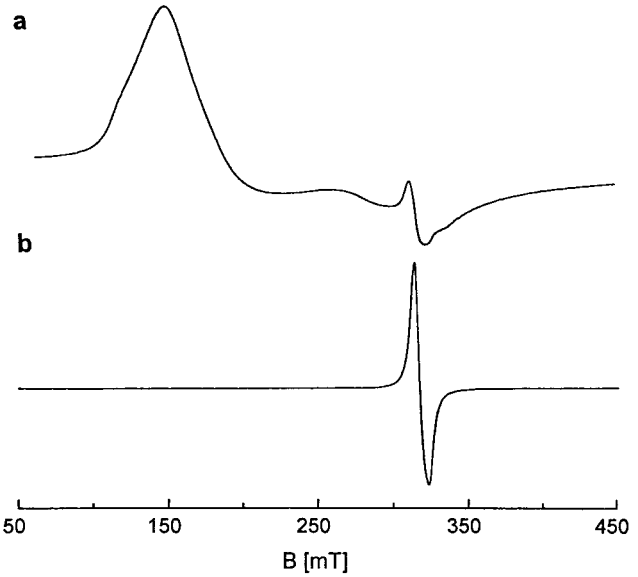

Figure 4. (a) EPR powder spectra of $[Ni^{III}Ni^{II}(\mathbf{3})][BPh_4]_2$ (**5b**) and (b) $[Fe^{III}Fe^{II}(\mathbf{3})][BPh_4]_2$ (**6b**) at 77 K. Conditions: microwave frequency, $\nu = 9.02$ GHz; microwave power, 2 mW (**5b**), 5 mW (**6b**); modulation frequency, 100 kHz; modulation amplitude, 4 G. Concentrations: (a) **5b**, 38 mg of Ni^{III}/1.0 g of sample (3.8%); (b) **6b**, 37 mg of Fe^{III}/1.0 g of sample (3.7%).

a similar feature is also found for $[Fe^{III}Fe^{II}(\mathbf{3})]^{2+}$ (**6b**), however, at a lower wavelength at 1280 nm ($\epsilon = 532$ M^{-1} cm^{-1}, fwhm = 2065 cm^{-1}). Since these bands are absent in the spectra of the fully reduced and oxidized Fe^{II}_2 and Fe^{III}_2 forms, these bands are assigned as intervalence transitions (IT).[61]

Heterodinuclear Complexes. Figure S8 (Supporting Information) shows the electronic absorption spectra of heterodinuclear complexes **7** and **8**. The UV−vis spectra of these two compounds are also similar but not identical, with two strong absorptions around 460 ($\epsilon \approx 2200$) and 610 nm ($\epsilon \approx 600$). Note that the low-energy bands exhibit long tails which extend into the region 950−1100 nm ($\epsilon \approx 70$ at 900 nm). Albeit the complexes are thought to contain discrete Co^{III} and Ni^{II} ions, the spectra are not simple superpositions of the spectra of complexes $[Co^{III}_2(\mathbf{3})]^{3+}$ and $[Ni^{II}_2(\mathbf{3})]^{+}$, presumably because of the strong dependence of the position of the CT bands on the number of M^{III} ions in the $[M_2(\mathbf{3})]^{n+}$ species. In fact, the spectra of **7** and **8** show more similarity to a hypothetical spectrum obtained by superposition of the spectra of $[Co^{III}Co^{II}(\mathbf{3})]^{2+}$ and $[Ni^{II}_2(\mathbf{3})]^{+}$. The strong absorption bands at 460 and 610 nm are then readily assigned as ligand-to-Co^{III} charge-transfer bands, and the weak absorptions in the 900−1000 nm region arise from d−d transitions of an octahedral $Ni^{II}N_3S_3$ chromophore.

EPR Spectra of 5b and 6b. The mixed-valent nature of complexes $[Ni^{III}Ni^{II}(\mathbf{3})][BPh_4]_2$ (**5b**) and $[Fe^{III}Fe^{II}(\mathbf{3})][BPh_4]_2$ (**6b**) has been further confirmed by preliminary EPR measurements. Figure 4a displays the EPR spectrum of a powdered sample of **5b** at 77 K. It reveals an axial signal as the main component with estimated g values of $g_\perp < \sim 4.0$ and $g_\parallel > \sim 2.05$ indicative of an $S = {}^3/_2$ spin ground state. In this case $g_\parallel \approx 2$, $g_\perp \approx 2(S + {}^1/_2) = 4$ for $S = {}^3/_2$.[62] Similar axial $S = {}^3/_2$ signals were previously observed for **5a**[29] and other mixed-valent

(61) The position of the IT band of **6a** was found to be independent of the choice of the solvent: in CH_3CN at 1405 nm (432 M^{-1} cm^{-1}), in CH_3COCH_3 at 1405 nm (412 M^{-1} cm^{-1}).

(62) Pake, G. E.; Estle, T. L. *The Physical Principles of Electron Paramagnetic Resonance*, 2nd ed.; W. A. Benjamin Publ.: London, 1973; p 127.

Table 5. Metal−Metal Separations and Ground States in $Y_3M(\mu\text{-}X)_3MY_3$ Complexes[a]

complex	d(M···M) (Å)	donor set	ground state	ref
$[Fe^{2.5}{}_2(\mu\text{-}OH)_3(tmcn)_2]^{2+}$	2.51	FeN_3O_3	$S = {}^9/_2$	11, 12
$[Fe^{II}{}_2(\mu\text{-}Cl)_3(tmcn)_2]^{+}$	3.014(2)	$(hs)Fe^{II}N_3Cl_3$	$S = 4$	5
$[Fe^{III}{}_2(\mu\text{-}S_2)_3(tacn)_2]$	2.546(2)	$(ls)Fe^{III}N_3S_3$	$S = 0$	22
$[Fe^{III}{}_2(\mathbf{1})_3]^{3+}$ $(\mathbf{6a})^{3+}$	nd	FeN_3S_3	$S = 0$	28
$[Fe^{III}Fe^{II}(\mathbf{1})_3]^{2+}$ $(\mathbf{6a})^{2+}$	2.79(1)	FeN_3S_3	$S = {}^1/_2$	this work, 49
$[Fe^{III}Fe^{II}(\mathbf{3})]^{2+}$ $(\mathbf{6b})$	2.79(1)	FeN_3S_3	$S = {}^1/_2$	this work
$[Fe^{II}{}_2(\mu\text{-}SMe)_3(CO)_6]^{+}$	3.062(4)	$(ls)Fe^{II}S_3(CO)_3$	$S = 0$	68
$[Ru^{III}{}_2(\mu\text{-}SPh)_3(Cp^*)_2]^{+}$	2.630(1)	$(ls)Ru^{III}Cp^*S_3$	$S = 0$	66
$[Ru^{III}Ru^{II}(\mu\text{-}S^iPr_3)_3(Cp^*)_2]$	2.968(2)	$RuCp^*S_3$	$S = {}^1/_2$	65
$[Ru^{II}{}_2(\mu\text{-}SH)_3(PMePh_2)_5(SH)]$	3.371(3)	$(ls)Ru^{II}P_3S_3$ $(ls)Ru^{II}P_2S_4$	nd	66, 67

[a] Abbreviations: tacn = 1,4,7-triazacyclononane; tmcn = 1,4,7-trimethyl-1,4,7-triazacyclononane, Cp* = η^5-C_5Me_5, ls = low-spin, hs = high-spin, nd = not determined.

$Ni^{III}Ni^{II}$ amine−thiolate complexes.[14,19] The $S = {}^3/_2$ ground states of these complexes are attained by an intramolecular ferromagnetic exchange interaction between low-spin Ni^{III} ($S = {}^1/_2$) and Ni^{II} ($S = 1$) ions.[63] It is thus likely that a similar exchange interaction occurs in **5b**. It should be noted that the EPR spectrum of **5b** reveals a second signal at $g \approx 2.16$, which was not observed for **5a**. The origin of this $S = {}^1/_2$ signal is, however, unclear at present.

Figure 4b depicts the X-band EPR powder spectrum of the mixed-valent iron complex **6b** at 77 K. The room temperature EPR powder spectrum is very similar. Both spectra consist of a strong $S = {}^1/_2$ signal centered at $g_{av} \approx 2.05$. Apparently there are no further signals at lower field. The spectra suggest that the mixed-valent $Fe^{III}Fe^{II}$ complexes exhibit an $S = {}^1/_2$ spin ground state.[64]

It is appropriate at this stage to compare our preliminary EPR results with those reported for other face-sharing bioctahedral complexes of Fe and Ru with an even (d^5d^5, d^6d^6 configuration) or uneven number (d^5d^6) of metal d electrons (see Table 5). The thiolate-bridged $Ru^{III}Ru^{II}$ complex $[Cp^*Ru(\mu_2\text{-}S^iPr)_3RuCp^*]$ ($Cp^* = \eta^5$-C_5Me_5),[65] for example, exhibits an $S = {}^1/_2$ ground state. The observed metal−metal distance of this complex at 2.968(2) Å is intermediate between those of other Ru_2 complexes having three bridging thiolate ligands with a Ru−Ru single bond (e.g., $[Ru^{III}{}_2(\mu_2\text{-}SPh)_3(Cp^*)_2]^{+}$,[66] Ru−Ru = 2.630(1) Å) and without a Ru−Ru bond (e.g., $[Ru^{II}{}_2(\mu_2\text{-}SH)_3(PMePh_2)_5(SH)]$,[67] Ru···Ru = 3.371(3) Å). Similarly, the metal−metal distances in the diamagnetic $Fe^{III}{}_2$ and $Fe^{II}{}_2$ complexes $[(ls)Fe^{III}{}_2(\mu_2\text{-}S_2)_3(tacn)_2]$[22] and $[(ls)Fe^{II}{}_2(\mu_2\text{-}SMe)_3(CO)_6]^{+}$,[68] respectively, differ by 0.52 Å. Interestingly, the Fe−Fe distance of the $Fe^{III}Fe^{II}$ compound **6a** examined in this study also lies between those of the two homovalent iron complexes. Thus, similar to the ruthenium complexes, there seems to exist a correlation between the number of metal d electrons and the Fe−Fe distance in the iron thiolate complexes. However, in the absence of more detailed spectroscopic and structural data one can only speculate about the electronic structure of these dimers.

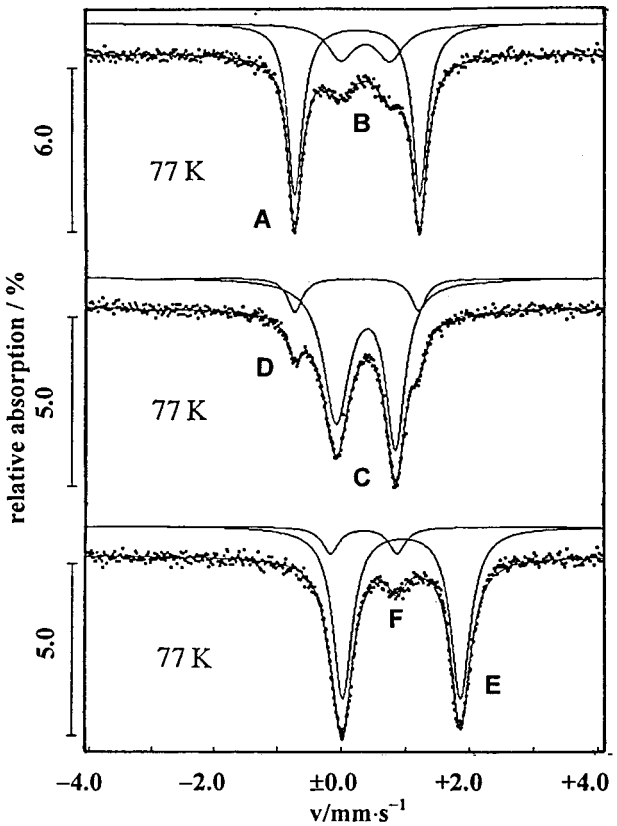

Figure 5. Zero-field ^{57}Fe Mössbauer spectra of $[Fe^{III}{}_2(\mathbf{1})_3]^{3+}$ (top), $[Fe^{III}Fe^{II}(\mathbf{1})_3]^{2+}$ (middle), and $[Fe^{II}{}_2(\mathbf{1})_3]^{3+}$ (bottom) at 77 K. The fits (solid lines) were obtained using the parameters listed in Table 6.

^{57}Fe Mössbauer Spectroscopy. Complexes $[Fe^{III}{}_2(\mathbf{1})_3]^{3+}$, $[Fe^{III}Fe^{II}(\mathbf{1})_3]^{2+}$, and $[Fe^{II}{}_2(\mathbf{1})_3]^{+}$ have also been preliminary characterized by ^{57}Fe Mössbauer spectroscopic measurements to investigate the possibility of electron delocalization in the mixed-valent $Fe^{III}Fe^{II}$ complexes. The zero-field spectra of the respective complexes at 77 K are shown in Figure 5. Table 6 gives the corresponding Mössbauer parameters. In the following we will only briefly discuss the results of these studies.[45]

$[Fe^{III}{}_2(\mathbf{1})_3]^{3+}$. The Mössbauer spectroscopic data for this Fe^{III}-Fe^{III} complex have been reported previously.[28] At 77 K, this complex gives rise to two quadrupole doublets at $\delta = +0.35$ mm·s^{-1} ($|\Delta E_Q| = 1.94$ mm·s^{-1}, denoted subspectrum A) and at $\delta = +0.46$ mm·s^{-1} ($|\Delta E_Q| = 0.76$ mm·s^{-1}, denoted subspectrum B), respectively, with an intensity ratio of 0.72:0.27. The observed isomer shift (δ) and quadrupole splitting (ΔE_Q) parameters of the more intense subspectrum A are characteristic for low-spin ferric ions with a *fac*-N_3S_3 donor set. The trinuclear complexes $[LFe^{III}MFe^{III}L]^{n+}$ (M = Cr, Co, Fe,

(63) For **5a**, a value of $J \approx +85$ cm^{-1} has been determined by analysis of the temperature-dependent magnetic susceptibility data. The theoretical expression for the determination of the exchange coupling constant has been obtained by using the Heisenberg−Dirac−van Vleck (HDvV) model for dinuclear complexes, with $\mathbf{H} = -2J\mathbf{S}_1\cdot\mathbf{S}_2$, ($S_1 = 1$, $S_2 = {}^1/_2$), see: O'Connor, C. J. *Prog. Inorg. Chem.* **1982**, *29*, 203−83. These results will be reported in a subsequent paper.

(64) The 293 and 77 K EPR powder spectra of **6a** are very similar with an intense signal at $g \approx 2.05$ at both temperatures.

(65) Dev, S.; Mizobe, Y.; Hidai, M. *Inorg. Chem.* **1990**, *29*, 4797−801.
(66) Hidai, M.; Imagawa, K.; Cheng, G.; Mizobe, Y.; Wakatsuki, Y.; Yamazaki, H. *Chem. Lett.* **1986**, 1299−302.
(67) Osakada, K.; Yamamoto, T.; Yamamoto, A.; Takenaka, A.; Sasada, Y. *Inorg. Chim. Acta* **1985**, *105*, L9−L10.
(68) Schultz, A. J.; Eisenberg, R. *Inorg. Chem.* **1973**, *12*, 518−25.

Table 6. Mössbauer Parameters for Complexes $[Fe_2(\mathbf{1})_3]^{n+}$ ($n = 1-3$) at $T = 77$ K

complex	subspectrum	$\delta^{\alpha-Fe}$,[a] mm·s^{-1}	Γ,[b] mm·s^{-1}	ΔE_Q,[c] mm·s^{-1}	A_r, %[d]	F[e]
$[Fe^{III}_2(\mathbf{1})_3]^{3+}$	A[f]	+0.35	0.28	1.94	73	1.136
	B[f]	+0.46	0.51	0.76	27	
$[Fe^{III}Fe^{II}(\mathbf{1})_3]^{2+}$	C[g]	+0.49	0.47	0.89	86	1.190
	D[f] (≡A)	+0.34	0.30	1.91	14	
$[Fe^{II}_2(\mathbf{1})_3]^{3+}$	E[f]	+1.04	0.36	1.83	88	1.548
	F[g] (≡C)	+0.45	0.25	1.02	12	

[a] Isomer shift vs α-Fe at 295 K. [b] Full width at half-height. [c] Quadrupole splitting. [d] Line area relative to total area. [e] Normalized value of the χ^2 test. [f] Subspectrum fitted by symmetrical Lorentz functions, doublet. [g] Spectrum fitted by an asymmetric doublet, asymmetry parameters for C: $\Gamma_2/\Gamma_1 = 0.77$, $A_2/A_1 = 0.89$; Γ_1 and A_1 refer to the left line.

Ni; see Chart 5 for the structure of the ligand), for example, exhibit a central $[N_3Fe^{III}(\mu\text{-}S)_3M(\mu\text{-}S)_3Fe^{III}N_3]^{n+}$ core with *fac*-N_3S_3 coordination environments for the terminal iron ions. These complexes have been reported to contain low-spin ferric ions.[20,21] The isomer shifts and quadrupole splittings of these complexes and of $[Fe^{III}_2(\mathbf{1})_3]^{3+}$ (spectrum A) are all similar.[69]

$[Fe^{II}_2(\mathbf{1})_3]^{+}$. Mössbauer spectroscopic data for the diiron(II) complex $[Fe^{II}_2(\mathbf{1})_3]^{+}$ have not been reported previously. This complex shows a well-resolved quadrupole doublet at $\delta = +1.04$ mm·s^{-1} (denoted as E). The additional weak absorptions (denoted F) come from an impurity, and the intensity of this doublet increases if the sample is exposed to air. The main component of the spectrum, quadrupole doublet E, can be assigned to iron(II) in the high-spin state on the basis of the large isomer shift ($\delta = 1.04$ mm·s^{-1}) and the relatively large quadrupole splitting ($|\Delta E_Q| = 1.83$ mm·s^{-1}).[70-72] These values should be compared with those of the trinuclear complex $[LFe^{II}(ls)Cr^{III}Fe^{II}(ls)L]^{+}$, where the Fe^{II} ions are in a low-spin d^6 configuration ($\delta = +0.54$ mm·s^{-1}, $|\Delta E_Q| = 0.14$ mm·s^{-1}).

$[Fe^{III}Fe^{II}(\mathbf{1})_3]^{2+}$ (6a). The spectrum of $[Fe^{III}Fe^{II}(\mathbf{1})_3]^{2+}$ shows a well-resolved quadrupole doublet (denoted as C) with $\delta = +0.49$ mm·s^{-1} and $|\Delta E_Q| = 0.89$ mm·s^{-1} as the main component, indicating that the valence states and chemical environments of the two iron sites are identical. The Mössbauer parameters are intermediate between those of the fully reduced Fe^{II}_2 and fully oxidized Fe^{III}_2 complexes. It is noted that there are weaker absorptions (D) closely surrounding the major quadrupole doublet. This latter absorption D, however, is not due to the mixed-valent iron complex. It rather stems from an impurity of the starting material $[Fe^{III}_2(\mathbf{1})_3]^{3+}$, which remained in the sample due to its incomplete reduction.[73]

Inspection of the data in Table 6 and comparison of the three spectra in Figure 5 clearly reveal that the Mössbauer spectrum of the mixed-valent iron complex $[Fe^{III}Fe^{II}(\mathbf{1})_3]^{2+}$ is not a simple superposition of the spectra of the Fe^{II}_2 and Fe^{III}_2 complexes. This would have been expected for a hypothetical species $[Fe^{III}Fe^{II}(\mathbf{1})_3]^{2+}$ with a localized oxidation state distribution. The observation of a single quadrupole doublet clearly reveals that the two iron ions are indistinguishable on the time scale of a Mössbauer experiment (10^{-7} s) at 77 K. These results are also supported by the low-energy electronic transition at 1406 nm in the UV−vis spectrum of $[Fe^{III}Fe^{II}(\mathbf{1})_3]^{2+}$. We anticipate further Mössbauer spectroscopic studies as well as temperature-dependent magnetic susceptibility measurements to gain further insight into the electronic structures of the mixed-valent iron complexes.

Concluding Remarks

In the present study it was shown that the amine−thiolate ligand $H_3\mathbf{3}$, similar to $H_1\mathbf{1}$, supports the formation of bioctahedral face-sharing complexes with a central $N_3M(\mu_2\text{-}SR)_3MN_3$ core (M = Fe, Co, and Ni). Both ligands provide similar sets of donor atoms, and the properties of homodinuclear $[M_2(\mathbf{1})_3]^{n+}$ and $[M_2(\mathbf{3})]^{n+}$ species are very similar. There are, however, several differences between the two ligands; the most important may be summarized as follows:

(1) The $[M_2(\mathbf{3})]^{n+}$ species are thermodynamically and kinetically more stable than the $[M_2(\mathbf{1})_3]^{n+}$ species, because of a conformationally more restricted ligand backbone. The complex $[Ni^{III}(\mathbf{3})]^{3+}$, for example, is much more stable than $[Ni^{III}_2(\mathbf{1})_3]^{3+}$, and this has allowed the recording and characterization of the electronic absorption spectrum of a $N_3Ni^{III}(\mu_2\text{-}SR)_3Ni^{III}N_3$ chromophore.

(2) The study of mixed-valent complexes of $H_3\mathbf{3}$ provides further insight into their electronic structures, as the electronic properties of the N_3S_3M and N'_3S_3M sites are different from one another. The different positions of the intervalence transitions in complexes **6a** and **6b**, for example, clearly show a perturbation of their electronic structures upon changing the donor set from N_3S_3 to N'_3S_3.

(3) Similar to the $[M_2(\mathbf{1})_3]^{n+}$ complexes, the $[M_2(\mathbf{3})]^{n+}$ are redox-active and undergo two chemically and electrochemically reversible one-electron-transfer reactions without changing the overall dinuclear structure. This allows for an investigation of metal−metal interactions between different metal ions M, M′, because ligand $H_3\mathbf{3}$ has the advantage that it forms homo- and heterodinuclear complexes equally well.

Further studies in these laboratories will focus on the structural characterization of the $[M_2(\mathbf{3})]^{n+}$ species. We will also examine the possibility of preparing heterodinuclear complexes $[MM'(\mathbf{3})]^{n+}$ containing two labile transition metal ions, as for instance a $[NiFe(\mathbf{3})]^{n+}$ species.

Acknowledgment. This work was supported by fundings of the Deutsche Forschungsgemeinschaft (DFG) and the Fonds der Chemischen Industrie (FCI). B.K. thanks Prof. Dr. H. Vahrenkamp for his generous support. We also thank Prof. Dr. A. Müller (University of Bielefeld) for providing facilities for X-ray crystallographic measurements and are indebted to M. Schmidtmann for help in collecting the X-ray data.

Supporting Information Available: Figure S1 of the central $[N_3Co(\mu\text{-}SR)_3CoN_3]$ core in **4c**; Figures S2 and S3 of the 2D NMR spectra of **4b** and of **4a**; Figures S4−S8 of the electronic absorption spectra of homodinuclear complexes $[Ni_2(\mathbf{3})]^{n+}$, $[Co_2(\mathbf{3})]^{n+}$, and $[Fe_2(\mathbf{3})]^{n+}$, of mixed-valent complexes $[M_2(\mathbf{3})]^{2+}$ (M = Ni, Fe, Co) and $[Fe_2(\mathbf{1})_3]^{2+}$, and of heterodinuclear complexes **7** and **8** in DMF in the range 400−1600 nm. An X-ray crystallographic file for **4c**, in CIF format. This material is available free of charge via the Internet at http://pubs.acs.org.

IC990087T

(69) It should be noted that the other quadrupole doublet (subspectrum B) in the Mössbauer spectrum of $[Fe^{III}_2(\mathbf{1})_3]^{3+}$ is not due to an impurity. It was rather shown by temperature-variable Mössbauer spectroscopy that the intensity ratio of the two subspectra is temperature dependent (the intensity ratio of the two subspectra was found to be A:B = 0.42:58 at 298 K). We have tentatively assigned subspectrum B to a species, $[(hs)Fe^{III}_2(\mathbf{1})_3]^{3+}$, containing ferric ions in the high-spin state, see ref 28.

(70) Greenwood, N. N.; Gibb, T. C. *Mössbauer Spectroscopy*; Chapman and Hall: London, 1971.
(71) Bancroft, G. M.; Platt, R. H. *Adv. Inorg. Chem. Radiochem.* **1972**, *15*, 59−258.
(72) Karlin, K. D.; Lippard, S. J. *J. Am. Chem. Soc.* **1976**, *98*, 6951−7.
(73) We have obtained an analytically pure sample of **6a**. The Mössbauer spectrum of this sample consists of a single quadrupole doublet with parameters identical to those of spectrum C.